Rb-Sr sphalerite data and implications for the source and timing of Pb-Zn deposits at the Caledonian margin in Sweden

Alfred Larsson

Dissertations in Geology at Lund University,
Master's thesis, no 529
(45 hp/ECTS credits)

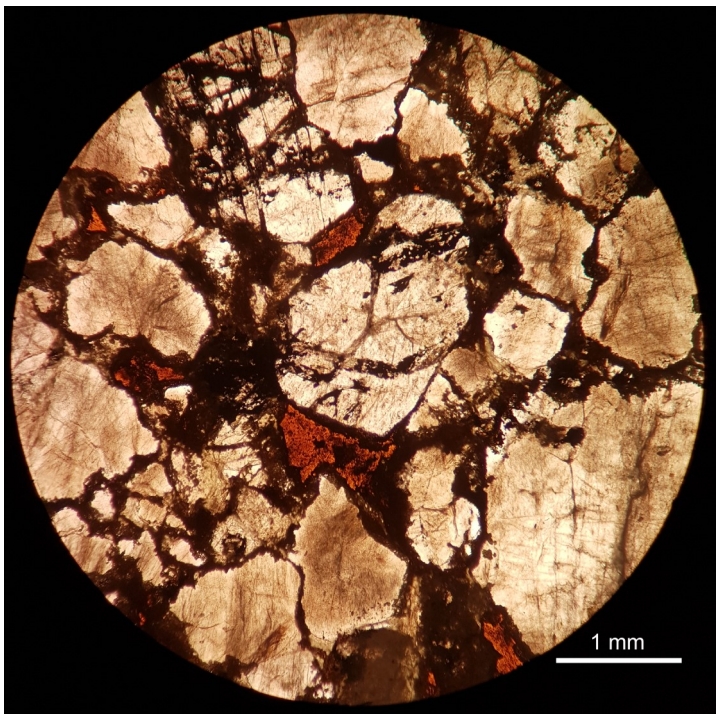

Department of Geology
Lund University
2018

Rb-Sr sphalerite data and implications for the source and timing of Pb-Zn deposits at the Caledonian margin in Sweden

Master's thesis
Alfred Larsson

Department of Geology
Lund University
2018

Contents

1 Introduction **7**
2 Geological setting **7**
2.1 Regional geology 7
2.2 Local geology at Laisvall and Granberget 8
3 Mineralization **9**
3.1 Sediment hosted Pb-Zn deposits 9
3.2 Mineralogy and mineralization style at Laisvall and Granberget 10
3.3 Previous models for ore genesis and ore controlling factors 12
4 Ore geochronology **13**
4.1 Dating mineralization and ore-forming processes 13
4.2 Application of the Rb-Sr dating technique 13
5 Methodology **15**
5.1 Principles of ID-TIMS 15
5.2 Purpose of Rb-Sr isotope analysis 16
5.3 Step-by-step description of sample preparation 16
5.3.1 Crushing of samples and separation of sphalerite 16
5.3.2 Heavy liquid separation 16
5.3.3 Washing and grinding of samples 16
5.3.4 Separation of leachate from residual sphalerite 17
5.3.5 Addition of $^{84}Sr/^{87}Rb$ mixed spike to the sample 17
5.3.6 Ion exchange procedure: collecting Rb, -Sr and -Pb eluates 17
5.3.7 Measurement of isotope ratios 17
5.4 Age calculations and error considerations 17
5.4.1 Estimation of blank 17
5.4.2 Mass-spectrometry 18
5.4.3 Calculations 18
6 Analytical results **18**
6.1 Rb-Sr isotope data 18
7 Discussion **21**
7.1 The possibility of a post-mineralization disturbance affecting the Rb-Sr system 21
7.2 The possibility of syn-ore processes creating heterogenities in Sr initial isotope values 21
7.3 Fluid mixing and ore-forming processes 22
7.4 Age estimates and possible genetic links between ores of different types 23
8 Conclusion **24**
9 Acknowledgements **25**
10 References **25**
11 Appendix **28**

Cover Picture: Sample BRB119 from Granberget, mineralized by sphalerite and galena. Photograph by Alfred Larsson.

Abstract

ALFRED LARSSON

Larsson, A., 2018: Rb-Sr sphalerite data and implications for the source and timing of Pb-Zn deposits at the Caledonian margin in Sweden. *Dissertations in Geology at Lund University*, No. 529, 34 pp. 45 hp (45 ECTS credits).

Abstract: The eastern Caledonian erosional front hosts the world-class Pb-Zn deposit at Laisvall (64 Mt mined) and Granberget mineralization, northern Sweden, along with several other smaller, related types of deposits consisting of impregnation mineralization of galena and sphalerite in clastic host rocks. Previous work have discussed the nature of the ore-forming processes and constraints for the timing of the mineralization, however, the mechanisms are still not fully understood and previous age determinations are ambiguous. The main challenge with obtaining reliable ages for the mineralization is the lack of minerals available for dating and the complex nature of the available isotope data. This thesis aims to improve the understanding for the ore-forming processes in the Laisvall type of deposit and, if possible, obtain an age for the mineralization by utilizing the crush-leach technique on disseminated sphalerite from Laisvall and Granberget with subsequent ID-TIMS isotope analysis. In general, the data is complex and our results does not provide a robust age for the mineralization. However, our data are in agreement with the hypothesis that ore-fluids with contrasting $^{87}Sr/^{86}Sr$ were mixing during the syn-ore forming stage. These results are opposing previous hypotheses which are favoring a post-ore disturbance causing scatter in the isotope data. Our data provide further support for hydrothermal circulation in response to orogenic tectonics at a regional scale, forming Pb-Zn mineralizations at multiple locations during a relatively short time-interval, either related to an event at ca. 540 Ma (related to the Timian orogeny) or at ca. 467 Ma (related to the Caledonian orogeny). Thus, these findings implicate that the Pb-Zn deposits in the Caledonian forefront was caused by a single, regional process. The results provide further insights to the genetic model for the Caledonian sediment hosted Pb-Zn deposits.

Keywords: Laisvall, Granberget, geochronology, sphalerite, ore, Rb-Sr

Supervisors: Kjell Billström (Swedish Museum of Natural History), Anders Scherstén (Lund University)

Subject: Bedrock Geology

Alfred Larsson, Department of Geology, Lund University, Sölvegatan 12, SE-223 62 Lund, Sweden.
E-mail: alfred.larsson999@gmail.com

Sammanfattning

ALFRED LARSSON

Larsson, A., 2018: Rb-Sr sphalerite data and implications for the source and timing of Pb-Zn deposits at the Caledonian margin in Sweden. *Examensarbeten i geologi vid Lunds universitet*, Nr. 529, 34 sid. 45 hp.

Sammanfattning: Längs Kaledonidernas östra erosionsfront finns den världskända bly- och zinkfyndigheten vid Laisvall (totalt 64 miljoner ton bruten malm) och mineraliseringen vid Granberget samt flertalet mindre malmkroppar av impregnationstyp bestående av blyglans och zinkblände som kristalliserat i klastiska bergarter. I äldre litteratur har mineraliseringsprocesserna och tidsspannet för mineralisationen diskuterats, men processerna är fortfarande långt ifrån klargjorda och tidigare dateringar bör beaktas med viss skepsis. Den huvudsakliga utmaningen med att producera pålitliga dateringar av malmen är dels avsaknaden av daterbara mineral och dels det komplexa mönstret hos den data som befintliga geokronologiska metoder producerat. Målet med denna uppsats är att klargöra och fördjupa förståelsen för malmbildningsprocesserna vid Laisvall- och Granbergetmalmerna samt, om möjligt, datera malmen med hjälp av ID-TIMS isotopanalys av rubidium och strontium från zinkblände. Datan är överlag komplex och svårtolkad och våra resultat kan inte ge en precis och robust ålder för mineraliseringen. Datan styrker däremot hypotesen om att malmfluider med kontrasterande $^{87}Sr/^{86}Sr$-isotopskvoter blandades i samband med malmgenesen. Dessa resultat står i motsats till tidigare hypoteser som argumenterar för att isotopsystemet skall ha blivit stört efter mineraliseringen avslutades. Vår data stödjer hypotesen om att bergskedjebildning kan ha gett upphov till hydrotermala fluider som cirkulerade på en regional nivå, vilket i sin tur ledde till bly- och zinkmineraliseringar på flertalet platser under ett relativt kort tidsintervall, relaterat till antingen den Timiska orogenesen (ca. 540 miljoner år sedan) eller ett tidigt stadium av den Kaledonska orogenesen (ca. 470 miljoner år sedan). Dessa resultat tyder på att bly- och zinkfyndigheterna längs den Kaledoniska bergskedjans rand har skapats av en ensam, regional process. I tillägg till detta bidrar också resultaten till en ökad kunskap och förståelse för Kaledoniska bly- och zinkmalmer i sedimentära moderbergarter.

Nyckelord: Laisvall, Granberget, geokronologi, zinkblände, malm, Rb-Sr

Handledare: Kjell Billström (Naturhistoriska Riksmuseet), Anders Scherstén (Lunds universitet)

Ämnesinriktning: Berggrundsgeologi

Alfred Larsson, Geologiska institutionen, Lunds Universitet, Sölvegatan 12, 223 62 Lund, Sverige.
E-post: alfred.larsson999@gmail.com

1 Introduction

The world-class sandstone hosted Pb-Zn sulphide-impregnation deposit at Laisvall (64.3 Mt at 4.0 wt. % Pb, 0.6 wt. % Zn, and 9.0 g/t Ag) is one of several clastic dominated sediment hosted lead-zinc ores (e.g. Granberget, Vassbo, Osen and Torneträsk) found in the present-day erosional front of the eastern Scandinavian Caledonides (Fig. 1) (Grip 1954; Rickard et al. 1979; Willdén 1980; Saintilan et al. 2015a). The Laisvall type of epigenetic, strata-controlled, funnel-shaped ore body (Saintilan et al. 2015b) has been considered to be a sub-category of the Mississippi-Valley (MVT) style of mineralization (Saintilan et al. 2015b) and similar deposits have been recognized in other parts of the world, e.g. the Jinding deposit, China of 200 Mt at 6.1 wt. % Zn and 1.3 wt. % Pb (Chi et al. 2005; Xue et al. 2007). The mineralization at Laisvall was discovered in 1939 and the mining operation was initiated in 1941 (Grip 1954), and proceeded until the operation was terminated in 2001 (Saintilan et al. 2015a). The mineralization consists of disseminated galena and sphalerite with minor abundance of calcite, fluorite, barite and pyrite, which forms an epigenetic cement that fills the interstitial volumes and parts of the sandstone grains (Grip 1954; Roedder 1968; Rickard et al. 1979; Romer 1992). The siliciclastic sedimentary sequence of paleoaquifers hosting the ore partly consists of autochtonous sandstone beds resting unconformably on the deeply eroded Proterozoic crystalline basement rocks and partly of allochtonous sediments in the lowermost units of the Caledonian thrust nappes (Grip 1954; Christofferson et al. 1979; Willdén 1980; Saintilan et al. 2015b). The regionally extensive Alum Shale Formation comprises the cap rock for the paleoaquifers and the disseminated galena and sphalerite mineralization (Christofferson et al. 1979; Willdén 1980; Saintilan et al. 2015b).

The lack of an absolute date for the mineralizing processes remains as one of the main causes for debate regarding the genesis for the ore at Laisvall and surrounding deposits. The age-interval for the mineralizing event is constrained by the maximum age of ca. 600 Ma for the diagenesis of the hosting sandstones and a minimum age of 400 Ma as the mineralization is considered to pre-date the Caledonian orogenesis due to the presence of reverse faults and occasional incorporation of mineralization in the lowermost allochthonous thrust sheets (Rickard et al. 1979; Saintilan et al. 2015a; Saintilan et al. 2015b). Recent Rb-Sr dating of sphalerite on crush-leachates has yielded a Middle Ordovician isochron age of 467 ± 5 Ma (MSWD = 1.4) for the ore-forming processes at Laisvall (Saintilan et al. 2015a). Due to the relatively small sample set this age is to be considered as preliminary. Attempts to date sphalerite in the vicinity of the Caledonian decollement at Laisvall and Granberget failed, and this was explained as due to perturbation of the Rb -Sr system caused by post-mineralization percolation of Sr-rich fluids (Saintilan et al. 2015a). Other Pb-Zn-mineralized breccia and vein deposits in the neighboring Lycksele-Storuman ore district have been tentatively dated to 535 ± 13 Ma with Rb-Sr on sphalerite (Billstrom et al. 2012).

The aim of this study is to refine and review the genesis and previous absolute age-determinations for the ore-forming event(s) of the Laisvall-type deposits using the crush-leach technique and ID-TIMS on a larger sample set. Another objective of this study has been to study the mineralogy and textures, in particular for samples selected for further isotope work. The geochronological data attained in this study will be discussed in the light of previous literature and put into geological context for further enhancing the genetic model of the Laisvall-type deposit. The industry has stressed the importance of improving the exploration model for sandstone hosted Pb-Zn ore deposits in the Scandinavian Caledonides for finding additional resources with similar style of mineralization (Saintilan 2015). In conjunction with previous work, this study aims to contribute to the understanding of sandstone hosted Pb-Zn deposits and improve exploration efforts for such deposits in the Scandinavian Caledonides and across the globe.

2 Geological setting

2.1 Regional geology

The Laisvall and Granberget Pb-Zn deposits are located in northwestern Sweden at the base of the Caledonian deformation front. The Laisvall mine area is located ca. 38 km west of the city of Arjeplog and the Granberget deposit ca. 250 km southwest of Laisvall in the Dorotea district (Fig. 1). The two deposits are part of a

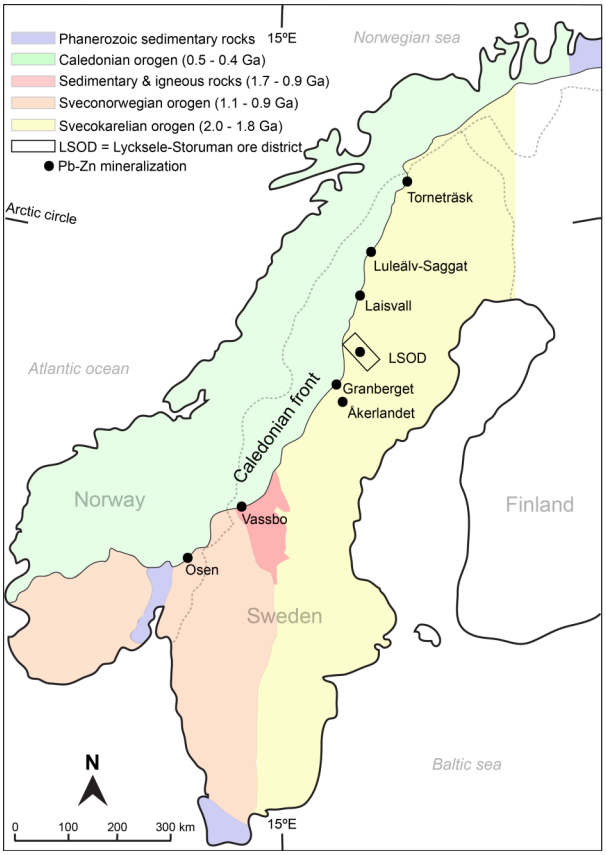

Fig. 1. Generalized bedrock map of Norway and Sweden. Black dots marks location for major Pb-Zn deposits along the Caledonian front. Modified after Rickard et al. (1979); Lindblom (1986); Gee et al. (2010); Saintilan et al. (2015a); Saintilan et al. (2015b).

series of similar, sandstone-hosted Pb-Zn deposits following the Eastern margin of the Caledonides and occasionally extend into the basement (Rickard et al. 1979). Another Pb-Zn type of mineralization occurs as mineralized vein and breccia deposits (e.g. Åkerlandet and the Lycksele-Storuman district) which occur exclusively in basement rocks (Fig. 1).

The studied deposits lie within the northwestern part of the Fennoscandian shield, which comprises large parts of Sweden, Norway, Finland and northwest Russia. The paleocontinent has commonly been denoted as 'Baltica' in paleogeographic literature. The crystalline basement rocks within the Fennoscandian shield in this region are of late Paleoproterozoic age 1.96–1.8 Ga (Stephens et al. 1994) and associated with the Svecokarelian orogeny. Subsequently, sedimentation and igneous activity (1.7–0.9 Ga), ceasing in the late Neoproterozoic (Saintilan et al. 2015a), affected the bedrock. The cratonic bedrock of Fennoscandia shows a trend of successively younger ages towards the southwest and is overlaid by a thin succession of largely eroded autochtonous sandstones and shales of Ediacaran to lower Cambrian and locally through lower Ordovician age (Willdén 1980; Moczydlowska et al. 2001). The sediments were deposited on the western stable platformal margin of Fennoscandia during the opening of the Iapetus Ocean and are unconformably superimposed on the deeply eroded bedrock (Grip 1954; Rickard et al. 1979; Saintilan 2015). The partly strongly deformed organic rich (10–20 wt. % carbon) Alum Shale Formation was deposited on top of the autochtonous sandstones, forming the central decollement and shear plane for the overthrusting nappes in the later Caledonian orogeny (Grip 1954; Gee 1975; Roberts & Gee 1985; Stephens 1988; Gee et al. 2010; Saintilan et al. 2015b).

During the early stages of the Caledonian orogeny (upper Cambrian and lower Ordovician) Baltica collided with a volcanic arc from the west, and subsequently subducted beneath Laurentia as the Iapetus Ocean was closing (Dallmeyer & Gee 1986). This resulted in the development of a foreland basin (Gee 1975; Stephens 1988; Gee et al. 2010; Saintilan et al. 2016a). The mineralization at Laisvall is constrained to Ediacaran and lower Cambrian sedimentary rocks, whereas an assortment of high grade metamorphic rocks, arc-related crustal material and exotic continental sequences are found further towards the northwest. The latter allochtonous units were thrusted onto Baltica in the east and are presently overlying the Alum Shale Formation (Gee 1975; Roberts & Gee 1985; Stephens 1988; Gee et al. 2010; Saintilan et al. 2015a; Saintilan et al. 2015b). These multiple Caledonian thrust sheets are divided into the Lower Allochthon situated in the Laisvall area, and the Middle and Upper Allochthons located farther to the west (Fig. 2) (Gee et al. 2010; Saintilan et al. 2015b).

2.2 Local geology at Laisvall and Granberget

The strata-bound Pb-Zn deposit type of Laisvall is hosted by the autochthonous Ediacaran to Lower Cambrian sedimentary rocks overlying the granitic bedrock (Fig. 3) (Christofferson et al. 1979; Rickard et al. 1979). The bedrock is fractured by regional north-northwest and north-northeast striking basement faults, controlled by older fault zones (Romer 1992). Several sets of joints have fractured the ore-bearing sandstone horizons in a pattern parallel to the regional basement (Grip 1954; Rickard et al. 1979; Romer 1992). The autochthonous sedimentary strata is in total ca. 100 m thick and is resting unconformably on the weathered Paleoproterozoic bedrock (Saintilan et al. 2015a). The autochthonous sequence is divided into the Ediacaran to Lower Cambrian Laisberg Formation (ca. 60 m thick) and the barren late Lower Cambrian Grammajukku Formation (ca. 40 m thick) comprised of interlayered shales and siltstones (Rickard et al. 1979; Willdén 1980; Nielsen & Schovsbo 2011). The Ediacaran units of the Laisberg Formation are composed of polymict, irregular conglomerate and sandstones overlain by pebbly shales (Rickard et al. 1979). The Cambrian units of the Laisberg Formation are subdivided into the Lower Sandstone ore horizon (also referred to

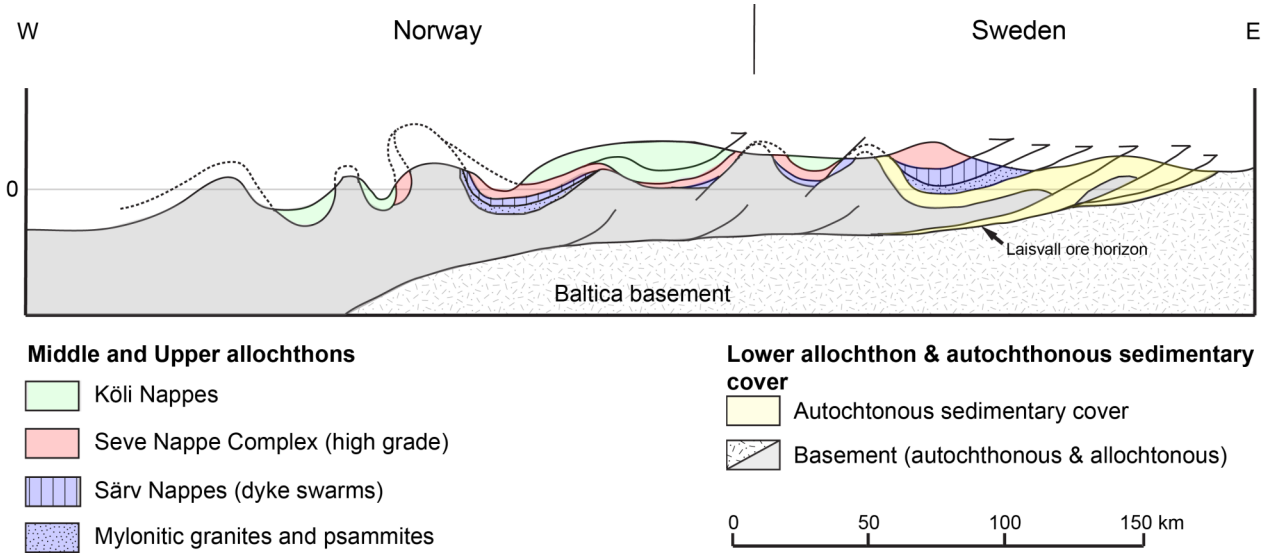

Fig. 2. Schematic cross-section of the major tectonostratigraphic units in the central Caledonides. The Laisvall mineralization is located in the autochthonous sedimentary cover in the east. Vertical exaggeration is 5x. Modified after Gee et al. (2010) and Saintilan et al. (2015a).

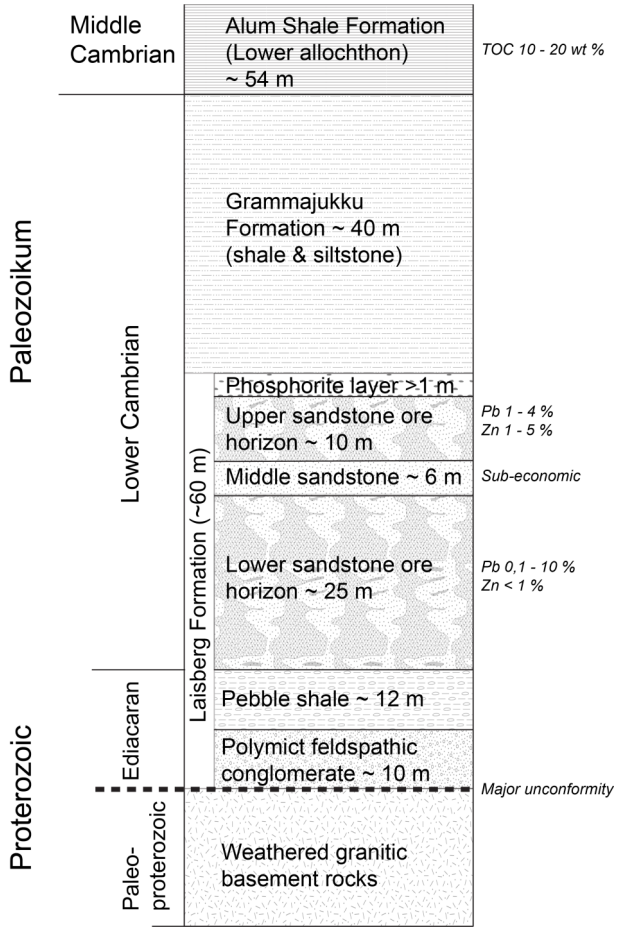

Fig. 3. Stratigraphic column of the autochthonous stratigraphic sequence at Laisvall. The sedimentary cover is resting unconformably on the Paleoproterozoic basement. The Total Organic Carbon (TOC) of the Alum Shale Formation is 10–20 wt. %. Average Pb and Zn grades are displayed by corresponding ore body. Modified after Rickard et al. (1979); Willdén (1980); Nielsen & Schovsbo (2011); Saintilan et al. (2015a)

as Kautsky member, 25 m thick), Middle Sandstone (Tjalek member, sub-economic, 7 m thick), Upper Sandstone ore horizon (Nadok member, 11 m thick) (Rickard et al. 1979; Nielsen & Schovsbo 2011; Saintilan et al. 2015b). The Lower Sandstone is a well-sorted, medium grained white sandstone interlayered with millimeter thin clay layers, flasers and occasional tidal bundles. The sub-economic Middle Sandstone is a medium grained grey, clay-rich sandstone with a basal thin, quartz conglomerate. The Upper Sandstone is a dark grey sandstone with tidal influences interlayered with siltstone and 5–15 cm thick repeated units of upward-decreasing grain-size (Willdén 1980; Casanova 2010). The autochtonous sequence at Laisvall is terminated with the Grammajukku Formation that is superimposed by the locally strongly deformed, black, organic rich Alum Shale Formation (ca. 54 m thick) at the base of the Caledonian thrust nappes (Ljungner 1950; Rickard et al. 1979).

The depositional environment for the Laisvall Formation has been interpreted as an early transgressional shelf-lagoon, subsequently affected by tidal currents forming alterations of clay-rich, coarse- and fine-grained sediments, eventually transforming into a beach setting with shallow lagoons depositing the Upper Sandstone horizon (Rickard et al. 1979; Nielsen & Schovsbo 2011). Thin phosphorite layers, commonly related with limestone lenses, were deposited onto of the Upper Sandstone Formation as a result of lagoonal sediment accumulation (Rickard et al. 1979).

The barren, autochthonous strata of Granberget are composed of shales and siltstones and are locally less than 10 m thick. In contrast to Laisvall, the autochthonous stratigraphy at Granberget lacks the characteristic porous, well sorted, white sandstones. The mineralization at Granberget is restricted to the Lower allochtonous units of the Caledonian nappes and is hosted by coarse-grained clast-supported sandstones and conglomerates (Saintilan et al. 2015a).

3 Mineralization

3.1 Sediment hosted Pb-Zn deposits

Pb-Zn deposits without immediate association with igneous activity hosted in sedimentary strata are denoted as sediment hosted Pb-Zn deposits (Leach et al. 2001; Leach et al. 2010). Within this group, individual deposits may show significant differences in geological factors such as tectonic setting, host rock composition, mineralization style, geochemistry, geology and precipitation processes. Commonly, the sediment hosted Pb-Zn deposits are further subdivided into two major subtypes: the sedimentary exhalative (SEDEX) and Mississippi-Valley type (MVT). Pb-Zn ores formed through expelling of ore-bearing hydrothermal solutions into a water reservoir, forming laminated, stratiform Zn-Pb-Ba (± Ag, Au, Cu, W and Bi) ores are traditionally referred to as SEDEX-deposits (Leach et al. 2005). MVT deposits typically form in carbonate rocks on basin flanks and foreland thrust belts from saline (10–30 wt. % salt), relatively low fluid temperatures (75–200 ºC) basinal brines, and are controlled by fractures and lithological transitions (Leach & Sangster 1993; Leach et al. 2005; Leach & Taylor 2009). However, a single deposit can show transitional features in between those typical for the SEDEX- and the MVT-style. There are also other terms used for sediment-hosted Pb-Zn mineralizations and for instance Bjørlykke & Sangster (1981) introduced the concept of sandstone-hosted deposits in which they grouped e.g. the Laisvall ore. Following the suggestion of Saintilan (2015), Laisvall and Granberget will be classified as a MVT-subtype in this thesis.

MVT deposits were first recognized by Bastin (1939) in the famous ore district of Mississippi River, Central US, as strata-bound, epigenetic, sulphide bodies (Paradis et al. 2007). The world's combined MVT-deposits account for roughly 25 % of the Pb and Zn resources in total (Paradis et al. 2007). The deposits are commonly comparatively small (avg. 7 Mt at ca. 7.9 % Pb and Zn combined), but tend to occur as clusters in extensive districts and are often distinguished on the basis of ore assemblages, mineralization controls, alteration, host rock and geochemical features where each district share similar characteristics in e.g. mineralogy and metal proportions (Leach et al. 2005; Leach & Taylor 2009; Saintilan 2015). The main

commodities are Pb and Zn but by-products can include e.g. Ag and Cu (Leach & Taylor 2009). The bulk of the MVT deposits are hosted in carbonate rocks although other (e.g. Laisvall deposit, Sweden and Jinding deposit, China) are present in clastic-dominated settings such as shales, siltstones and sandstones (Leach et al. 2005; Leach et al. 2010; Saintilan et al. 2016a).

The major factors discriminating sandstone hosted Pb-Zn of Laisvall subtype from the generic MVT-deposit is that the host rock is not carbonate but sandstone, Pb dominates over Zn and the mineralization forms a disseminated, mottled, epigenic cement. Ore minerals are primarily epigenetically mineralized galena and sphalerite, cementing the interstitial porespaces between quartz and feldspars in the sandstone at Laisvall.

3.2 Mineralogy and mineralization style at Laisvall and Granberget

The economic mineralization is strictly strata-bound and restricted to the two paleoaquifers of the Lower and Upper Sandstone (Fig. 4). The ore bodies are composed of two thin, elongate sandstone units gently dipping to the west-northwest interlayered by the barren Middle Sandstone (Grip 1954; Rickard et al. 1979). Sharp crosscutting contacts with the country rock are present in the southeast, while the ore body fades out diffusively to the northwest and is confined by an elevated bedrock section in the northeast (Rickard et al. 1979). The Lower sandstone is ca. 5000 m long and 200 to 600 m wide and ranging from 2 to 24 m in thickness (Fig. 5). The Upper sandstone is smaller: ca. 2000 m long, 300 m wide and 2 to 8 m thick.

In general, the ore-bearing horizons at Laisvall follow the moderately undulating bedrock surface and are largely undisturbed with the exception of two major reverse faults, the Nadok and Kautsky faults (Rickard et al. 1979; Saintilan et al. 2015a). The Lower and Upper Sandstones are locally truncated by steeply dipping sphalerite-galena-calcite veinlets (Rickard et al. 1979; Saintilan et al. 2015b). The highest ore-grades are found in the coarse-grained sandstones with minor clay content and mineralized intervals are strictly controlled by the sedimentary properties of the hosting sandstone (Grip 1954; Rickard et al. 1979). The Lower Sandstone is lead dominated

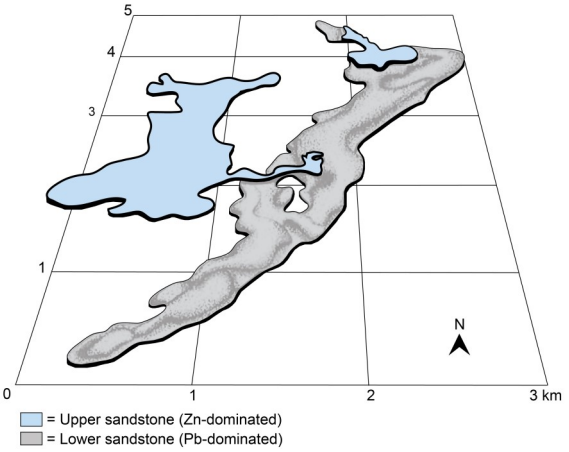

Fig. 5. Three dimensional model of the Laisvall mineralization with the Pb-dominated Lower sandstone orebody (grey) and the Zn-dominated Upper sandstone orebody (blue). Both orebodies have their major elongation axes in a 40º NE direction. Modified from Rickard et al. (1979).

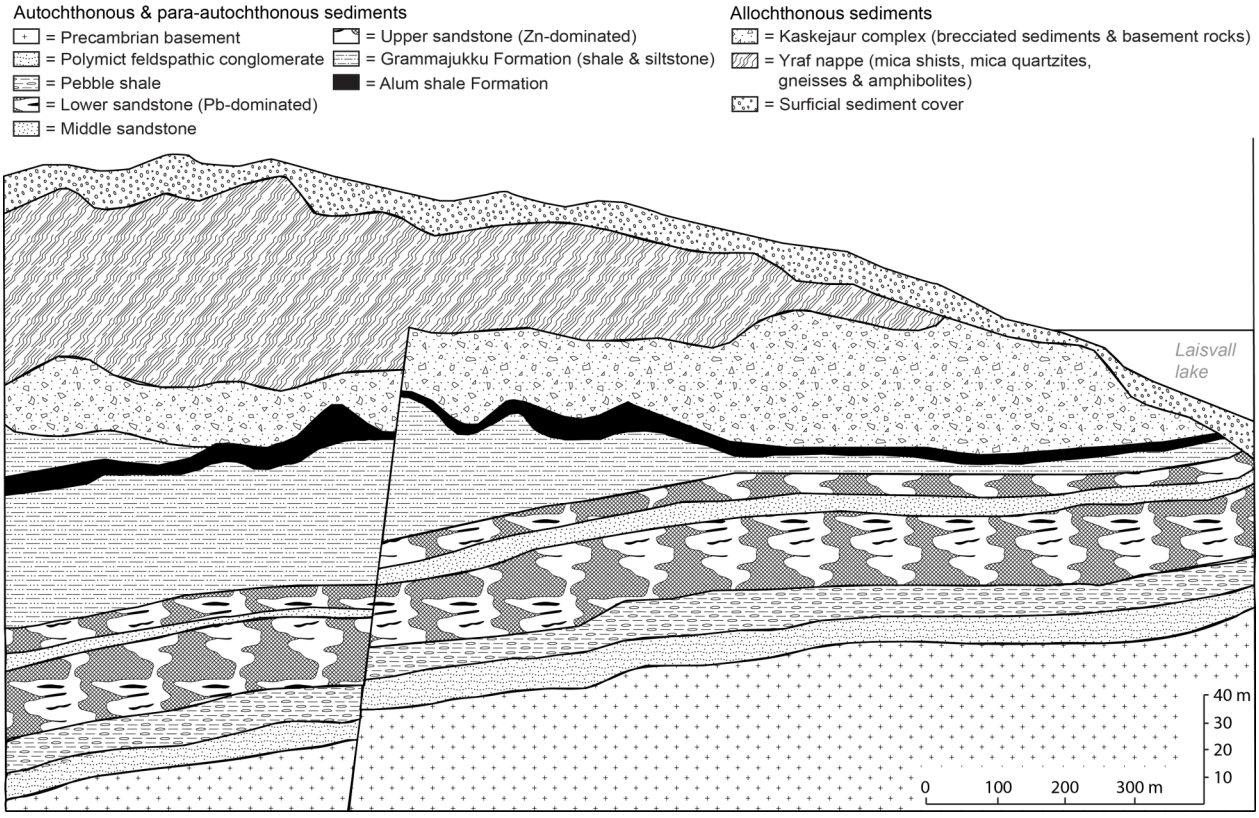

Fig. 4. Schematic cross-section of the Laisvall mine area. Vertical scale is exaggerated. Modified after Rickard et al. (1979).

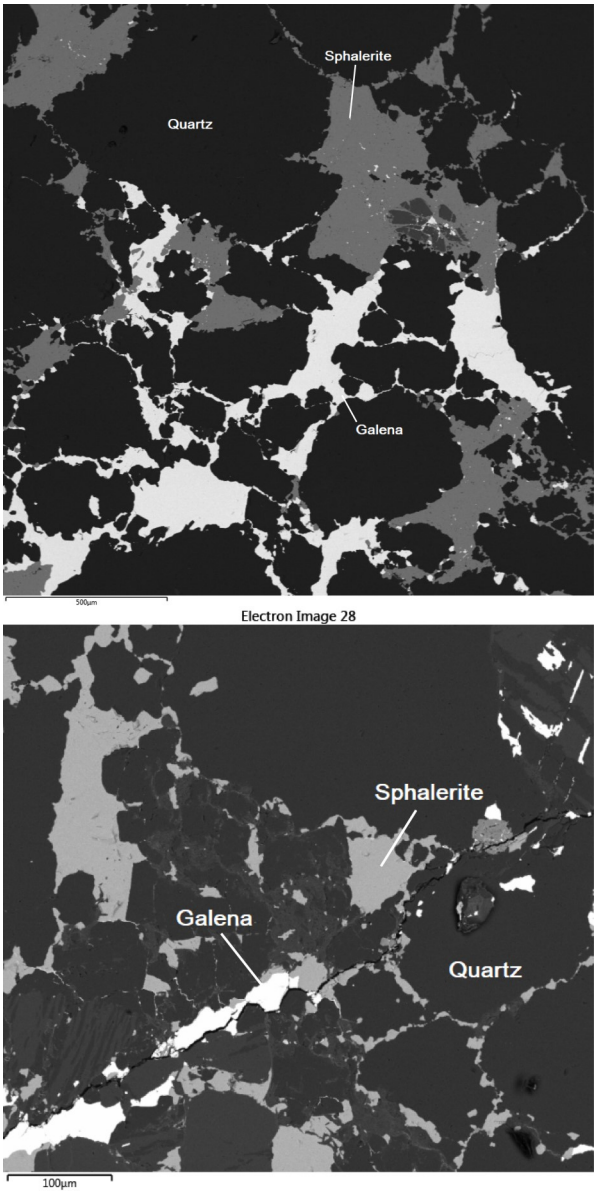

Fig. 6. Back-scatter electron image of sample Lai Bh 1203 (upper) and Granberget 02-09 (lower). Note the disseminated galena (white) and sphalerite (grey), cementing the interstitial spaces between the quartz grains.

with Pb grades varying between 0.1–10 wt. % and Zn grades being < 1 wt. %. In contrast, the Upper Sandstone is essentially Zn ore, dominated by sphalerite with a Zn grade of 1–5 wt. % and Pb-grades of 1–4 wt. % (although locally > 12 wt. % Pb) (Lindblom 1986; Saintilan et al. 2015b). Ore grades are fairly constant laterally but show a greater vertical variation due to the relative thin hosting sandstone bodies. In the southeastern parts of the deposit, the ore is concentrated to the Lower Sandstone but is gradually enriched at higher levels in the Upper Sandstone towards the northwest (Rickard et al. 1979).

The mineralogy of the Laisvall Formation sandstones is primarily composed of detrital quartz and locally seriticized K-feldspar (absent in Upper Sandstone) and with minor abundance of clay minerals, zircon, biotite, pyrite, monazite, organic compounds and occasional intergrown sphalerite-apatite (Saintilan et al. 2015b; Saintilan et al. 2016a). Galena and sphalerite are the only ore-minerals (Fig. 6), present as mottled, disseminated cement filling the interstitial volumes. Gangue minerals of pyrite, titanium oxides, fluorite, barite and calcite form a cement preceding the ore-cementation (Christofferson et al. 1979; Lindblom 1986; Saintilan et al. 2015a; Saintilan et al. 2016a). Flourapatite is present as an early diagenetic cement but also as a secondary, syngenetic generation (Saintilan et al. 2016a). Both detrital and hydrothermal monazite have been described in literature, occasionally with galena inclusions (Saintilan et al. 2016a). However, only a few single crystals (< 50 µm) of monazite were discovered using SEM-microscopy in the samples used in this study. The monazite grains were of insufficient quantity and size for U-Pb dating with laser ablation. Inclusions of galena in sphalerite indicate that formation of galena preceded sphalerite deposition. The sphalerite from Laisvall exhibits color variations ranging from honey yellow and greenish to orange and brown (Fig. 7). Moreover, sphalerite from the Lower Sandstone are distinguished from Upper Sandstone sphalerite by its lack of zoning, higher mean Fe-content and greater fluid inclusion homogenization temperatures (Lindblom 1986). Leaching textures have also been observed in sphalerite, demonstrating reversible processes and a hydrothermal system approaching equilibrium. At least three stages of sphalerite have been identified petrographically (Lindblom 1986), and these stages are characterized on the basis of color, zoning, inclusions, textural features and coating (Table. 1). Color zoning has mainly been identified in the Upper Sandstone while being absent in the Lower Sandstone. Iron content shows a greater variation (0.34–3.33 wt. %) in the Lower Sandstone than in the Upper Sandstone (0.15–0.65 wt. %), suggesting that there is no correlation between color and Fe-content (Lindblom 1986).

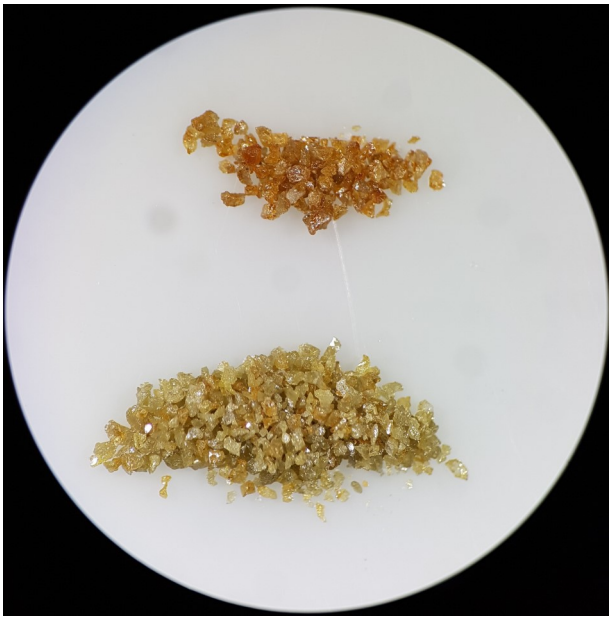

Fig. 7. Stereo micrographic image of the sand-sized sphalerite grains from sample Lv 04-09 (Laisvall) grouped by color.

Table 1. Three different generations of sphalerite and their respective characteristics. Compiled from Lindblom (1986).

Sphalerite stage	Colour Zoning	Growth zoning	Colour	Inclusions	Textual features
I	Not present	Oscillatory	Light yellow	Pyrite, galena	Nucleation on pyrite
II	Present	Banded zoning	Beige to brown	Hydrocarbon	Etched formed crystal surfaces
III	Present	Banded/sector zoning	Yellow to colourless	Hydrocarbon	Marked anisotropy

The mineralogy of Granberget resembles that of Laisvall: quartz and feldspar grains cemented by disseminated galena and sphalerite cut by galena-sphalerite-calcite veinlets. A number of thin-sections, 150 µm thick and originally prepared for fluid inclusions analyses, have been investigated in his study. Descriptions and images can be found in Appendix.

3.3 Previous models for ore genesis and ore controlling factors

The genesis of the Caledonian Pb-Zn mineralizations at Laisvall, Granberget, Osan and Vassbo have been debated and multiple models for ore controlling factors have been proposed. The Laisvall deposit has been in focus in particular. Bjørlykke & Sangster (1981) favored a syn-sedimentary model of metals carried by groundwater originating from the fractured and weathered basement, in a process driven by heat convection introduced from an underlying heat-producing granitic intrusion. Most other authors have stressed the epigenetic character of the sandstone hosted deposits. For instance Rickard et al. (1979) suggested a scenario where interaction between a metal-bearing solution and a highly saline, metal-poor sulfide-bearing fluid with a temperature of ca. 150 ºC, caused metals to precipitate in isotopic disequilibrium. They further proposed that temperature and pH were of less importance compared to the activity of reduced sulfur in the mineralizing process. Saintilan et al. (2015b) argued that reduced thermogenic sulfur supplied from gas traps in the uppermost parts of the paleo-aquifer was the key mechanism for precipitating the sulphide ore minerals. The driving force of the horizontal flowing brines may have been the compressive, thin-skinned Caledonian tectonics resulting in metal precipitation in the paleo-aquifer without any relationship between the ore and local tectonic structures (Fig. 8). In this scenario, the main factor controlling the geometry of the deposit is the permeability of the paleo-aquifer, based on observations of the varying ore grades correlating with variations in permeability in conjunction with the distribution of impermeable shale layers. Kendrick et al. (2005) argued for widespread basement interactions of two or more hydrothermal, basinal brines based on studies of noble gas isotopes and halogen contents in fluid inclusions. In conjunction with basement interactions, fluids were also likely to have been affected by circulation in areas rich in organic-rich matter that contributed reduced sulfur (Kendrick et al. 2005). Romer (1992) and Kendrick et al. (2005) discussed the role of pre-existing Proterozoic basement faults that were subsequently re-activated by the Caledonian tectonics, creating local areas of improved permeability through the basement rocks

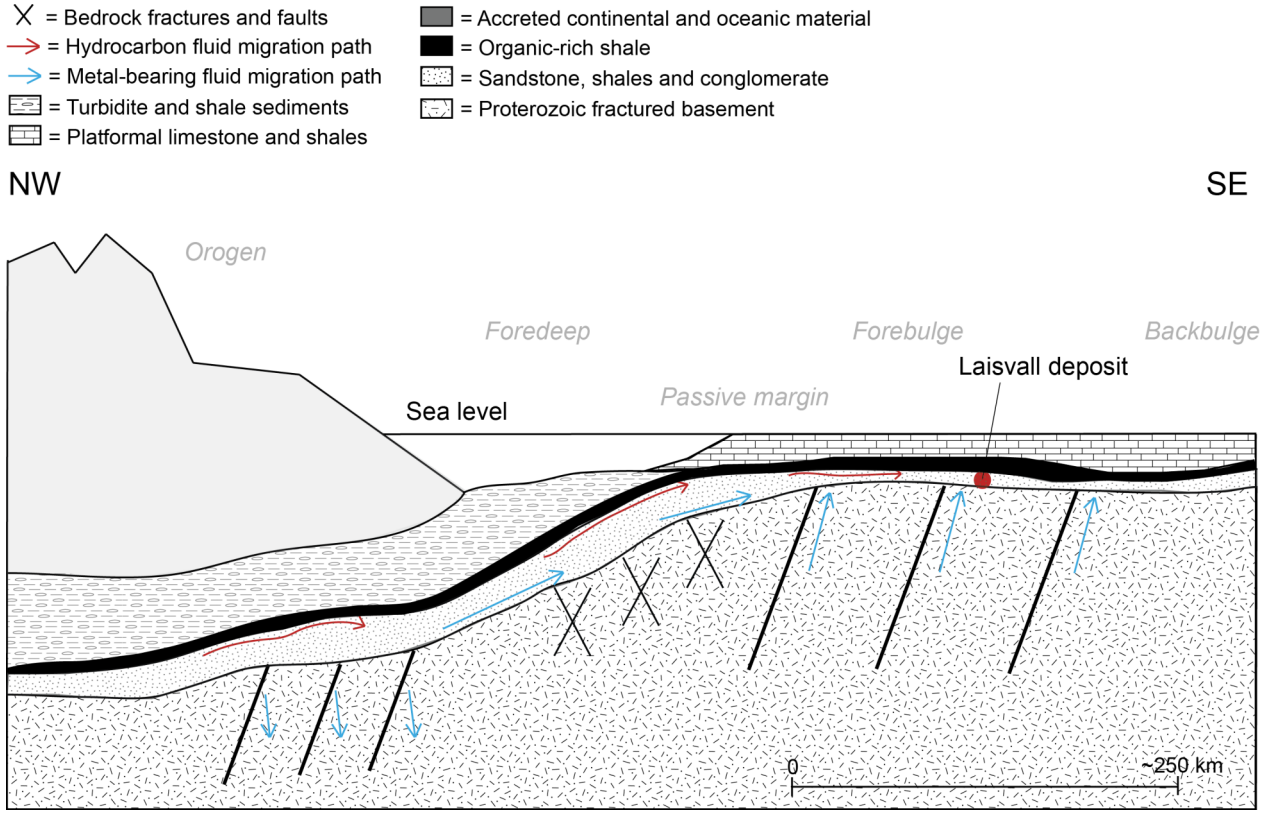

Fig. 8. Schematic model for the fluid flows involved in the mineralizing processes at Laisvall. Modified after Kendrick et al. (2005); Saintilan et al. (2015a)

and overlying Ediacaran-Cambrian units. The suggested primary fluid-controlling factor was basement faults acting as feeder channels for metal-bearing brines, whereas the sedimentary properties of the autochtonous strata exerted a secondary control (Romer 1992).

The Laisvall type deposit has been hypothesized (Saintilan et al. 2015a) to be genetically associated with vein hosted Pb-Zn deposits based on the mineralogical resemblance (calcite, fluorite, sphalerite and galena), their relative proximity to each other and geochronological data that could suggest synchronous origin. Tectonic structures associated with the vein hosted Pb-Zn deposits (e.g. Åkerlandet and others in the Lycksele-Storuman area) may have acted as feeder channels for metal rich brines supplied to the Laisvall deposit, possibly in multiple phases (Fig. 8) (Johansson & Rickard 1984; Saintilan et al. 2015a). Tentatively, the basement-hosted fluids protruded upwards and interacted with the superimposed paleoaquifers. Metals leached from the basement rocks were precipitated in the pore spaces as the highly saline brines mixed with cooler pre-existing fluids in the aquifer (Romer 1992). The basement-leaching model has been reinforced by airborne magnetic data, displaying magnetic lineaments correlating with faults and fractures in the autochthonous sedimentary rocks that have been interpreted to be extending into the basement (Saintilan et al. 2015b). Ore body-modelling of the Laisvall mineralization has displayed funnel-shaped geometry of the ores bodies with the highest grades in the proximity of the basement feeder-channels, further supporting their importance for metal transport and precipitation. Analysis of the spatial distribution of ore minerals show galena-mineralization present in the proximity of the basement faults and sphalerite mineralization forming a distal shell pattern (Saintilan et al. 2015b).

To summarize; most recent studies emphasize the role of re-activation of basement structures in the ore-forming processes responsible for the sediment-hosted, epigenetic Pb-Zn type of deposit. The similarities of the mineralization style at Laisvall and Granberget are hypothesized to be a consequence of regional scale tectonics and fluid migration, resulting in contemporaneous ore formation (Saintilan et al. 2015b).

4 Ore geochronology

4.1 Dating mineralization and ore-forming processes

Accurate and precise dating of ore deposits has historically been recognized to be particularly difficult, partly due to the lack of suitable dateable phases and partly to imperfections, such as very low closure temperatures inherent in certain radioactive systems. There are exceptions, such as the Re-Os system which does allow for direct dating of certain ore minerals. This geochronometer is particularly well suited for dating molybdenite, but this phase is not present in the studied mineralizations and when this technique is applied on other sulphides the necessary precision cannot always be obtained due to low Re-Os concentrations. A widely used approach for dating mineralizations is to date gangue minerals that are co-genetic (e.g. showing inter-grown mineral textures) with the mineralization. Yet, these results must be interpreted carefully since many ore deposits have a complex genesis and intricate relation with the host rocks e.g. leading to multiple generations of mineral growth. Another common method to determine the age of hydrothermal deposits is to date fluid inclusions inferred to be synchronous with the hydrothermal system forming the ore. Here other problems may arise, such as a dynamic hydrothermal system evolution, including fluid mixing, that could cause highly complex results (Dickin 2005).

There are a number of radiogenic isotope systems used in geochronology for isotopic dating of certain minerals which can be used directly or indirectly for dating ore-forming processes e.g. Sm-Nd, U-Pb, Re-Os, Lu-Hf, K-Ar, Ar-Ar and Pb-Pb. These systems are based on radioactive decay of a mother to daughter isotopes (in some systems through longer decay chains). The time passed since the closure of the specified mineral can be calculated using equations for radiogenic decay and empirically defined decay constants. Element diffusion is prevented in the crystal when the mineral cools below its closure temperature, whereby the radiogenic clock starts. However, some assumptions needs to be fulfilled for the radiometric date to reflect the true age of the formation of the mineral, and these are further discussed in context with the Rb-Sr system which is utilized in this work. First, the system must have remained closed (no gain or loss of mother or daughter elements) after reaching the closure temperature of the selected mineral type (Faure 1986). Rubidium and strontium for instance, are relatively mobile alkaline elements that could be easily mobilized if the mineral is sufficiently thermally or chemically altered. Metasomatic events such as percolating hydrothermal solutions or metamorphic fluids may disturb the system by initiating diffusion of the radiogenic isotopes which in turn will (partly or completely) disturb the system and thereby an erroneous age is obtained (Faure 1986; Attendorn 1997). Second, the initial isotopic ratio of the daughter element in the geochronometer (e.g. $^{87}Sr/^{86}Sr_{initial}$) must be consistent for the analyzed samples. In order to obtain a valid isochron, the analyzed sample sets are assumed to be co-genetic by sharing a common geological history and therefore have been affected by the same processes (e.g. crystallized from the same magma or precipitated from the same hydrothermal solution). This assumption is occasionally associated with problems. Ore minerals may form during multiple stages, re-equilibrate with magmas or hydrothermal solutions with other isotopic compositions than the one characterizing the initial stage, precipitate from a mixture of fluids with different compositions or simply by not being geologically related. Third, the dated minerals must be directly related to the mineralizing processes involved.

4.2 Application of the Rb-Sr dating technique

The first studies using Rb-Sr technique on sphalerite were published in the early 1990's (e.g. Nakai et al. 1990; Brannon et al. 1992; Nakai et al. 1993) and the method has since then been particularly used for da-

ting MVT-deposits (Saintilan et al. 2015a). The validity of the results obtained from this technique were initially questioned, but subsequent studies using Rb-Sr isotope systematics on sphalerite have yielded consistent results when compared to other geochronometers such as Re-Os (Selby et al. 2005; Schneider et al. 2007). The system relies on Rb and Sr, which are incompatible elements with Rb being more incompatible than Sr, resulting in relative enrichment of Rb vs. Sr in the fluid phase. Crustal rocks forming from residual melts will consequently be relatively enriched in Rb compared to Sr, resulting in elevated levels (radiogenic) of $^{87}Sr/^{86}Sr$ over time due to the radiogenic decay of ^{87}Rb to ^{87}Sr. Crustal rocks therefore have higher ratios of $^{87}Sr/^{86}Sr$ compared to depleted mantle rocks. In minerals other than sphalerite, Rb^{+} and Sr^{2+} commonly substitute for K^{+} and Ca^{2+}, respectively; however, Rb^{+} (1.52 Å, VI-coordination) and Sr^{2+} (1.18 Å, VI-coordination) are unlikely to substitute for Zn^{2+} (0,74 Å, VI-coordination) in the sphalerite crystal lattice due to the large difference in ionic radii (Nakai et al. 1993; Christensen et al. 1995). Substitution of Rb and Sr ions in sphalerite have previously been discussed to be a result of charge balanced coupled substitution $2Zn^{2+} \leftrightarrow Rb^{+} + Me^{3+}$ (e.g. Me = Sn, Sb or Ga) (Pettke & Diamond 1996). However, recent LA-ICPMS data (Saintilan et al. 2015a) on sphalerite have supported the hypothesis of Pettke & Diamond (1996) that Rb and Sr ions are sited in octahedral voids present in the sphalerite crystal lattice (Fig. 9) instead of being supplied from micro-inclusions. Rb and Sr are most likely incorporated into the octahedral voids during rapid crystal growth (Saintilan et al. 2015a).

The Rb-Sr isotopic dating system is based on the naturally occurring isotopes of ^{85}Rb and ^{87}Rb and ^{84}Sr, ^{86}Sr, ^{87}Sr and ^{88}Sr. The only radioactive isotope in this system is ^{87}Rb with a half-life of about 49.6 Ga which decays to ^{87}Sr through β^{-} decay (Villa et al. 2015). The ratio of $^{87}Rb/^{86}Sr$ decreases synchronously as the $^{87}Sr/^{86}Sr$-ratio is increasing, which is utilized when calculating the age of a mineral or rock. A Rb-containing mineral can be dated by calculating *t* using the decay constant for ^{87}Rb and the basic decay equation (1):

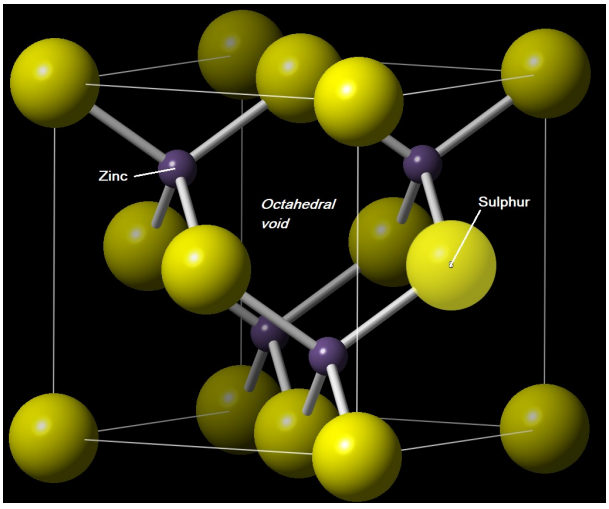

Fig. 9. Model of the sphalerite crystal structure. The octahedral voids hosting the lattice bound Rb and Sr is marked in the centre of the diagram.

$$(1)\ {}^{87}Sr = {}^{87}Sr_i + {}^{87}Rb\left(e^{\lambda t} - 1\right)$$

where *t* is the time passed since closure of the mineral, ^{87}Sr and ^{87}Rb are the measured present-day absolute abundances of atoms of each element in a unit weight, λ is the decay-constant of ^{87}Rb which is $1.3972\times10^{-11}a^{-1}$ (Villa et al. 2015) and $^{87}Sr_{initial}$ is the amount of ^{87}Sr at the time of mineral formation (Attendorn 1997). Mass-spectrometers measure *isotope ratios* (e.g. $^{87}Sr/^{86}Sr$) more precisely compared to absolute *isotope abundances*. Since ^{86}Sr is stable over time and is not produced by radioactive decay it can be used as a reference isotope. Each term in eq. (1) is simply divided by the number of atoms of ^{86}Sr, turning concentrations into measurable ratios in the age determination equation (2) displayed below (Dickin 2005):

$$(2)\ \left(\frac{{}^{87}Sr}{{}^{86}Sr}\right) = \left(\frac{{}^{87}Sr}{{}^{86}Sr}\right)_i + \left(\frac{{}^{87}Rb}{{}^{86}Sr}\right)\left(e^{\lambda t} - 1\right)$$

Absolute concentrations of ^{87}Rb and ^{87}Sr must be known for calculating *t,* which is done by measuring the absolute abundances of the respective element, either with isotope dilution (ID) mass-spectrometry or e.g. by x-ray fluorescence (XRF) and then applying equation (3) (Faure 1986; Attendorn 1997):

$$(3)\ \left(\frac{{}^{87}Rb}{{}^{86}Sr}\right) = \left(\frac{[Rb]}{[Sr]}\right) \times \left(\frac{{}^{87}Rb_{Ab}W_{Sr}}{{}^{86}Sr_{Ab}W_{Rb}}\right)$$

where $^{87}Rb/^{86}Sr$ is the absolute quantity of atoms in a given unit weight of the mineral, ([Rb]/[Sr]) is the concentration ratio of the elements, Ab refers to the element isotope abundance and W is the atomic mass of corresponding elements (Attendorn 1997). In practice, the samples are dissolved for producing a pure Sr salt through cation exchange chromatography, and subsequently the isotope ratio of $^{87}Sr/^{86}Sr$ of each individual sample is measured in a mass-spectrometer (Faure 1986). After extrapolating or assuming $^{87}Sr/^{86}Sr_{initial}$ and calculating $^{87}Rb/^{86}Sr$ from the Rb/Sr weight ratio, eq. (2) can be used for solving the parameter *t* (time). Equation (2) can be considered as a re-written version of the general equation for a straight line (4):

$$(4)\ y = c + mx$$

where $^{87}Sr/^{86}Sr$ (y) and $^{87}Rb/^{86}Sr$ (x) are the plotted ratios, $^{87}Sr/^{86}Sr_{initial}$ (c) is the intercept of the y-axis defining the initial $^{87}Sr/^{86}Sr$-ratio of the system and $e^{\lambda t}$ -1 (m) is the slope of the straight line, referred to as an isochron which represents the time *t* that has passed since sample crystallization (Faure 1986; Dickin 2005). The $^{87}Sr/^{86}Sr$ (y) and $^{87}Rb/^{86}Sr$ (x) values are plotted in an isochron diagram (Fig. 10). The validity of *t* is based on the assumptions that the system have remained closed with respect to Rb and Sr and that a satisfactory value of $^{87}Sr/^{86}Sr_{initial}$ is used. Thus, *t* will only be relevant as long as the geologic history is represented by the model of the analyzed co-genetic minerals, i.e. sharing the same age and the same initial Sr isotope composition (Attendorn 1997). The dates obtained from an assumed $^{87}Sr/^{86}Sr_{initial}$-value are com-

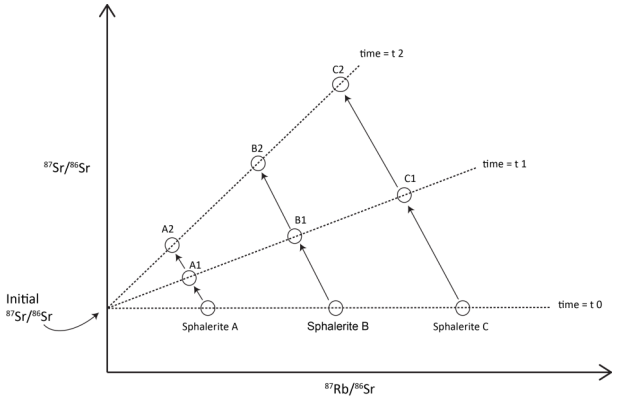

Fig. 10. Theoretical evolution of a perfect Rb-Sr system. The hypothetical sphalerite samples A, B and C do initially have the same $Sr^{87}/Sr^{86}_{initial}$ value but varying $^{87}Rb/^{86}Sr$. Assuming the system is closed, each sample will evolve as ^{87}Rb decays to ^{87}Sr. Theoretically, all samples will align on a regression line (isochron = same age) if the system remain undisturbed. Billström (personal communication).

monly referred to as "model-dates" in contrast to an isochron date which is obtained by extrapolating the line defined by individual sample points until it intersects the y-axis (Faure 1986). A hypothetical set of minerals forming from a magma or hydrothermal solution with homogeneous $^{87}Sr/^{86}Sr_{initial}$ and varying $^{87}Rb/^{86}Sr$ will initially (at time = t0) plot as a horizontal line in the Rb-Sr isochron diagram (Fig. 10) (Attendorn 1997). As the minerals cool below their closure temperature, diffusion is prevented and radiogenic ^{87}Sr will start accumulating from the decay of ^{87}Rb. Data points will move along straight lines with a slope of -1 since the increase of the $^{87}Sr/^{86}Sr$ isotope ratio will be of the same magnitude as that of the decrease in the $^{87}Rb/^{86}Sr$ isotope ratio (Fig. 10) (Dickin 2005). Although the data points successively will move in the diagram, their positions are at any given time constrained to a single, "rotating" straight line of which the slope value increases as a function of the time passed. As a result, the value of $^{87}Sr/^{86}Sr_{initial}$ remains unchanged irrespective of the length of time that has passed (assuming the system remains closed). In order to obtain a good-quality isochron, a considerable variation in $^{87}Rb/^{86}Sr$ (x-axis) is required, as this will ultimately determine the precision of the slope value of the isochron.

Once values of $^{87}Sr/^{86}Sr$ and $^{87}Rb/^{86}Sr$ for individual samples are obtained, an appropriate statistical procedure (e.g. least-squares regression) and computer software data reduction are used to align the data points to a best-fit straight line (isochron). As noted earlier, the slope of the line yields t from the relationship of the slope $e^{\lambda t}$-1 and the intersection with the y-axis yields the $^{87}Sr/^{86}Sr_{initial}$ value (Faure 1986). In real situations, there will always be an uncertainty in t as the linear fit will never become perfect and a certain data scatter is commonly observed. This is normally a combination of analytical errors, which never are insignificant, and geological errors arising due to e.g. a certain variability in the initial $^{87}Sr/^{86}Sr$ values expressed by individual samples, or to a mobility of rubidium or strontium taking place at a post-crystallization stage, or because all analyzed samples were not of the same age. (Attendorn 1997).

5 Methodology

5.1 Principles of ID-TIMS

The isotope dilution thermal ionization mass-spectrometry (ID-TIMS) is a high-precision technique generating isotope ratios. Isotope dilution is a method that allows the concentration of a selected element to be quantified with high precision and accuracy. This can be accomplished in a clean laboratory through a process often referred to as "spiking" in which a well characterized amount of tracer (typically a solution enriched in one of less abundant isotopes; ^{84}Sr isotope for Sr) is added to a sample of known weight. By acquiring certain isotope ratios involving e.g. the ^{84}Sr isotope, the concentration of Sr in the sample can be obtained. The actual mass spectrometric analysis allows both the isotope ratios of the sample to be obtained, as well as the element concentration – if the sample was spiked prior to analysis.

A TIMS instrument is based on the thermal ionization effect obtained through heating of a sample containing a single element until ionization of its atoms is achieved. The method requires that a chemical purification of the selected element, often obtained by ion chromatography, is applied prior to mass spectrometry. The TIMS technique is suitable for elements with relatively low first ionization potentials such as Sr or Pb but can be used for other elements as well. The instrument is composed of three main components: (1) the ion source (ion producer/accelerator), (2) the mass analyzer (discriminating isotopes by their mass/charge ratios) and (3) the detector (recording ion beams). Initially the purified sample is dissolved in an acid and mounted on a clean and outgassed filament. The latter is a thin ribbon often made of rhenium metal. The mounted sample is then carefully dried and loaded in the vacuum chamber of the mass-spectrometer. The sample is ionized by gradual heating of the filament by inducing an electric current. The operator can carefully monitor and regulate the ionization process by controlling the strength of the current (i.e. the heat of the filament). The filament emits excited species of the element that are focused into a single beam through a series of electrostatically charges plates. The ion beam is directed through an electrostatically induced magnetic field where mass discrimination occurs and the species are dispersed into multiple beams depending on their mass to charge ratio. For instance, if a strontium sample is loaded the detector system is set up to analyze single charged ions of the masses 84, 86, 87 and 88. Each ion beam is collected by a Faraday cup collector which converts the ion intensity to voltage that yield precise isotope ratios when signal ratios are compared to each other.

One of the main advantages with TIMS is the stability of the ion beam, which enables the precise measurement of isotope ratios. However, as the lighter masses ionise more efficiently than the heavier, the ratio between two isotopes of different masses changes over time. This effect results in mass dependent fractionation, which needs to be corrected for before plotting the data.

5.2 Purpose of Rb-Sr isotope analysis

The purpose of the analyses was to obtain an age for the formation of the Laisvall and Granberget ores by a direct-dating approach on sphalerite grains using the ^{87}Rb-^{87}Sr isotope system. Rubidium and strontium incorporated in the sphalerite crystal lattice should theoretically represent a closed system since the mineral crystallized, providing a suitable geochronometer.

A potential problem is that fluid inclusions present in sphalerite crystals may also contain strontium and rubidium. Fluid inclusions (from a few microns up to typically 50 microns) are small volumes of gas ± liquid, foreign mineral inclusions and salts that have become trapped in minerals. Some fluid inclusions may have been trapped at the same time as the host mineral crystallized, this type of fluid inclusion is not likely to present any analytical challenge as they, hypothetically, contains the same initial type of strontium as the component bound to voids in the crystal lattice. However, there may also exist other fluid inclusion types of a secondary origin that were introduced at a later event. Thus, in case a sphalerite sample is directly dissolved in acids, there is risk that Sr from mixed sources is analyzed, which would generate misleading age information. Thus, in order to date the mineralizing processes forming the sphalerite, the solid sphalerite material needs to be separated and liberated from possible interfering fluid inclusions.

Isotope analysis of elements contained within fluid inclusions may yield valuable geological information about e.g. the fluid composition and hydrothermal system, fluid source, ore forming stages and possible relations to other deposits. For these reasons, both a residual phase (referred to as the R-fraction and corresponding to strontium and rubidium related to voids in the sphalerite structure and therefore assumed to reflect the situation at the primary crystallization), and leachates (referred to as the L-fraction and corresponding to strontium and rubidium in fluid inclusions) may be analyzed separately. Thus, there is a need to split a sample into two sub-fractions, which is done by very careful grinding of the sphalerite sample (weighing from a few milligrams to about 30 milligrams in this study) using a specially designed boron carbide mortar comprising a very hard surface. Further details of this procedure are given below – see section 5.3 below.

As noted earlier, the mass spectrometry requires pure samples and there is thus a need to separate Rb and Sr from the other elements making up sphalerite. Therefore, the samples need to undergo an ion exchange procedure in order to separate and purify each element. The principle is to treat R and L fractions individually, and separate the specified elements in columns filled with an ion exchange resin. Strontium and rubidium can be separated through passing the dissolved samples through an ion exchange resin. Certain resins have affinity for specific elements, which will form a strong complex with the resin, while other elements flow through. For a given resin type, the molarity and choice of acid determines if a specific element forms a complex with the resin and remain there or travels (slowly or rapidly) through the resin and can be collected.

The concept of "spiking" was introduced earlier, and in the clean lab the spiking procedure takes place prior to the ion exchange step. Since the calculation of a Rb-Sr date requires that the concentration of both Sr and Rb are known, a mixed $^{84}Sr/^{87}Rb$ tracer was added to the R and L fractions selected for analysis. The sample-spike mixture is analyzed in a mass-spectrometer, yielding the mixed isotopic composition expressed in abundance ratios, which can subsequently be utilized for calculating the element concentrations in the sample solution.

5.3 Step-by-step description of sample preparation

Washing and grinding of samples were done in a clean lab with atmospheric overpressure. Crucial steps with high risk for contamination were carried out in air-flow secured fume hoods. Acids used were of high purity and the water used was of MilliQ quality (resistivity about 18.2 MΩ cm). Containers and pipettes were thoroughly pre-cleaned in acid.

5.3.1 Crushing of samples and separation of sphalerite

A stainless-steel hammer and solid metal anvil block were covered in thick aluminum foil for avoiding cross-contamination of samples. The samples were crushed to fine sand-sized particles and the material was inspected in stereo-microscope for determining its character and to define the pureness, grain size and color of the sphalerite. Grain size separation was required after the samples had been crushed for obtaining a grain size suitable for sphalerite separation. For most samples, gravitational separation through carefully shaking of the sample on a white paper in conjunction with sieving using 350–100 μm mesh size was sufficient. The actual picking of sphalerite grains was also done under a stereo-microscope. Only pure sphalerite grains were selected to obtain aliquots of 10–20 mg sphalerite.

5.3.2 Heavy liquid separation

Some samples comprised a fine-grained mix of different mineral phases, requiring heavy liquid separation in order to separate the sphalerite. Such samples were initially washed with water, dried and then centrifuged in test-tubes filled with the heavy liquid LST (approximate density is 2.95 g/cm^3), separating the grains into a heavy, sphalerite rich fraction and a gangue fraction. The sphalerite-dominated fraction was separated by freezing the heavy fraction in liquid nitrogen, and subsequently thawn and isolated from the light liquid. The heavy liquid was removed from mineral grains in a glass system equipped with a filter and a vacuum pump. The sphalerite fraction was transferred to a Petri dish and prepared for further sphalerite separation and picking.

5.3.3 Washing and grinding of samples

The samples were washed with water and leached in 2M HCl and 2M HF while being ultrasonicated. The samples were then washed repeatedly with water to remove as much as possible of traces of acids that may contain minor concentrations of the elements of interest. The clean separates were added, one by one in a small volume of clean water, to the pre-cleaned boron carbide mortar. The samples were grinded thoroughly

for ca. 3 minutes in deionized water. The intention is to produce a sample that is fine-grained enough to ensure that all fluid inclusions were liberated. The samples, now in the form of very fine-grained solid material as well as a fluid part carrying elements liberated from fluid inclusions, were transferred to centrifuge-tubes when completely grinded.

The mortar and pestle was cleaned repeatedly by ultrasonicating it in water for a few minutes between handling each sample. The mortar and pestle were further cleaned by placing them in concentrated HNO_3 for 15 minutes and then rinsed repeatedly.

5.3.4 Separation of leachate from residual sphalerite

The centrifuge-tubes containing the grinded samples were shaken, rinsed with water and centrifuged repeatedly. The solid, fine-grained residual sphalerite was kept in the bottom of the test-tube while the leachate was extracted to other containers. The R-samples were washed repeatedly with 2M HCL and 2M HF under ultrasonification for 10 minutes respectively. The samples were then centrifuged and washed with deionized water repeatedly to minimize the effect from traces of acids may have on the relevant isotopic compositions. Finally, the R-samples were transferred to clean and pre-weighed Teflon vials, and after drying they were weighed once again to produce the weight of the residual fraction. The weight of the L-samples cannot be estimated as the size or number of liberated fluid inclusions remain unknown, which will make concentration estimates highly uncertain while isotopic ratios are unaffected.

5.3.5 Addition of $^{84}Sr/^{87}Rb$ mixed spike to the sample

A few drops of spike solution were added to each sample respectively and the Teflon vial was weighed before and after spike addition. The spiked samples were put in aluminum cases and left on hot plates at ca. 130 ^{o}C to dry, after which 6M HCl was added to each sample. The containers were repeatedly opened to avoid pressure build-up of H_2S in the containers and then allowed to cool overnight. A large part of sample Lv 04-09 was accidently lost, possibly due to H_2S build-up. Because no smell of H_2S was present during a previous inspection, the sample-spike equilibration reaction was assumed to be complete. This, in conjunction with element concentrations within the normal range provide further justification for the assumption that the spike had equilibrated with the sample prior to volume loss and that the isotopic results from this sample are trustworthy.

5.3.6 Ion exchange procedure: collecting Rb, -Sr and -Pb eluates

A combination of different ion exchange steps are required in order to produce element solutions that are clean enough to yield good results during the mass spectrometric analyses. Two types of resin (True-Spec + Sr-Spec that help to isolate e.g. iron and strontium, respectively, from the elements of interest) were mixed and added to pre-cleaned Teflon micro-columns. The columns were repeatedly washed with 6M HCl and FC31 (0.3 M HF – 0.1 M HCl) and then conditioned with 6M HCl. Next, each sample (dissolved in 6 M HCl) was added to separate micro-columns and a combined Rb and Sr solution, free from elements such as U and Fe, was collected. Subsequently, Rb was collected from each sample, and the respective solution was allowed to dry. Following this, Sr was collected through adding heated 0.05M HNO_3 to the micro-columns.

Any Ba present was separated from the Sr fraction in the following step, and the previously collected Rb fractions had to go through a second purification step. Basically, these separation steps followed the principles outlined above. These final steps also involved the collection of Pb from the R-samples, which made it possible to also analyze Pb isotopes in sphalerite. However, these type of analyses were not part of the present work and will be discussed elsewhere.

5.3.7 Measurement of isotope ratios

The Rb-samples were dissolved and loaded on a double-filament setup. The Sr-samples were loaded on a single-filament setup and a BTA-activator solution was added to offset the high ionization potential of strontium. All isotope ratio measurements were done on a Thermo-Fisher Triton Mass-Spectrometer. The process is semi-automated, but the operator needs to monitor the behavior of each sample, as the ionization may take place at different rates and is dependent on e.g. variable sample sizes. The general idea is to start the measurements when signal intensities are high enough to produce stable and precise isotope ratios and then collect data for a time period long enough to allow the implementation of statistical treatment of data.

5.4 Age calculations and error considerations

Radiometric ages can be calculated following the procedures discussed when the general equations for radiogenic decay were previously introduced (see section ‘Ore geochronology’). Once Rb and Sr concentrations and the appropriate Rb and Sr isotope ratios are available, Rb-Sr isochron ages can be calculated with a software program. However, it is important to realize that such an age has uncertainties. There are a number of errors involved in the treatment of data and these are briefly mentioned below.

5.4.1 Estimation of blank

There may be minor traces of e.g. Sr and Rb in the acids, water, resins and Teflon ware etc. that are used during the course of lab treatment. Their effect on the final isotopic results obtained when the samples are analyzed can be corrected for by carrying out a blank measurement. This means that the very small effect of the laboratory contamination is quantified by treating a “blind” sample, i.e. a complete analysis (dissolution, spiking, isotope measurements, etc.) is carried out using a Teflon vial without any added mineral sample. Eventually, the blind sample is ready for mass spectrometry and ideally (zero contamination) the measured ratios will fully resemble those of the added spike. In reality, the deviation between measured ratios and known spike ratios are used to quantify the effect of the lab contamination. Generally, the ion exchange

procedure used for separating Rb and Sr in "conventional" mineral and rock samples (normally much larger sample sizes are involved) implies very low blank (contamination) levels in the picogram range. However, it is hard to fully quantify the absolute blank levels for crush-leach samples as it is difficult to mimic the procedures involved in the crush-leach step. Nevertheless, reasonable total blank levels for Rb (2 pg) and Sr (10 pg) were used in the software program utilized for the data reduction.

Also, the ^{84}Sr spike is not totally clean in the sense that it contains ^{84}Sr atoms exclusively. Such a spike has, however, been thoroughly calibrated with respect to the concentration of various Sr isotopes, but there are yet uncertainties in these estimates.

5.4.2 Mass-spectrometry

A large range of smaller and larger uncertainties are introduced during a run. The most important effect, which was mentioned before, is mass fractionation. This concept is quite complicated and involves issues such as normalization and standardization. In this context it is enough to stress the importance of analyzing primary standards (having known isotopic compositions) along with secondary standards which yield an estimation of the accuracy of the results. There are also a number of other sources of errors such as background noise and isobaric interferences which are normally not of any major concern when running Rb and Sr samples as the software is taking account of their influence on obtained ratios.

5.4.3 Calculations

Certain Excel spread-sheets (Ludvig 2001) are tailored for calculating Rb-Sr isochron ages. The operator enters estimated errors for each of the parameter values that are required as input data. These individual errors are propagated such that a total, combined error in the x- ($^{87}Rb/^{86}Sr$) and y-values ($^{87}Sr/^{86}Sr$), respectively, is defined. The net effect is that a regression with the purpose of aligning sample points will be characterized by a slope value that also has errors, which reflect the errors of individual points. The very final result is that the software can calculate an isochron age with an assigned error that matches the overall uncertainties in fitting individual data points to a line.

The older decay constant for ^{87}Rb of $1.42*10^{-11}a^{-1}$ (Steiger & Jäger 1977) was used for the isochron calculations in this paper in order to enable a comparison between the isotope data obtained in this paper and older data such as Saintilan et al. (2015a). When using the decay constant of Villa et al. (2015), all obtained ages become ca. 2 % older which should be kept in mind when interpreting the results.

6 Analytical results

6.1 Rb-Sr isotope data

Analytical Rb-Sr isotope data obtained in this study have been combined with previous Rb-Sr data from Laisvall and Granberget performed on residual sphalerite by Saintilan et al. (2015a) and is presented in Fig. 11 and Table 2. The data represent five series based on location and mineralization style as follows: (1) "Laisvall Upper sandstone disseminated sphalerite", (2) "Laisvall Lower sandstone disseminated sphalerite", (3) "Laisvall Upper sandstone sphalerite veinlet", (4) Laisvall Lower Sandstone sphalerite veinlet" and (5) "Granberget disseminated sphalerite". In general, the isotope data for the residual sphalerite from Laisvall and Granberget ore bodies are scattered. $^{87}Rb/^{86}Sr$ isotope data for disseminated sphalerite in the Laisvall Upper Sandstone range between 0.082–13.15, Laisvall Lower Sandstone range between 0.49–7.25 and Granberget ranges between 0.14–30.15, respectively. In contrast, the $^{87}Rb/^{86}Sr$ isotope data from Laisvall Upper Sandstone Veinlet and Laisvall Lower Sandstone Veinlet range between 0.16–0.26 and 0.26–0.47 respectively. The majority of the $^{87}Sr/^{86}Sr$ isotope values are moderately radiogenic, ranging between 0.718 and 0.776, with four samples yielding highly radiogenic $^{87}Sr/^{86}Sr$ values (> 0.800). As a result of the highly variable $^{87}Rb/^{86}Sr$ ratios, the variation in $^{87}Sr/^{86}Sr$ isotope data is large; with a total range for the entire dataset between about 0.718 and 0.949 (Fig. 11). Furthermore, sphalerite residues with brown colour from Granberget deposit tend to have higher $^{87}Rb/^{86}Sr$ values compared to their counterparts.

The leachate isotope data display significantly less overall spread in $^{87}Rb/^{86}Sr$ (0.07 to 1.55) compared to the residual sample data, with most data below 0.20 (Fig. 12 and Table 3). Yet, there is a large range in the leachate $^{87}Sr/^{86}Sr$ isotope data, from 0.718 to 0.745. Almost all leachates from the Laisvall sandstone veinlet series, the Granberget disseminated series, and two of the Laisvall Upper sandstone disseminated samples plot along an almost vertical array indicating low and similar $^{87}Rb/^{86}Sr$ isotope ratios. In contrast, the Laisvall Lower sandstone disseminated samples, in particular, have significantly higher $^{87}Rb/^{86}Sr$ isotope ratios (Fig. 12).

Saintilan et al. (2015a) used three residual sphalerite samples of a disseminated style from the Lower sandstone at Laisvall to calculate their isochron age of 467 ± 5 Ma (MSWD = 1.4). Sample LAQ 176 from the same ore horizon (this study) plots relatively close to the 467 Ma isochron and its incorporation in a regression (n = 4) pertaining to the Lower sandstone yields an age of 465 ± 22 Ma and an initial Sr isotope ratio of 0.716 ± 0.0011 (Fig. 11) (MSWD = 91). That is, the added point does not significantly change the earlier suggested age, but the precision of the age and the quality of the "isochron" becomes lower. Additional data from the present study scatter considerably and cannot be used to constrain or support the suggested 467 Ma age, and basically no well-defined isochron can be fitted to any of the data series. However, a crude linear array may be fitted to four of the residual samples from Granberget (see regression line in Fig. 11) yielding an imprecise date of 508 ± 48 Ma (MSWD = 97) and an indicated Sr isotope intercept of ca 0.732 ± 0.008. There are also other arrays that can be constructed which, however, are based on fewer samples and associated with very high (>1000) MSWD values.

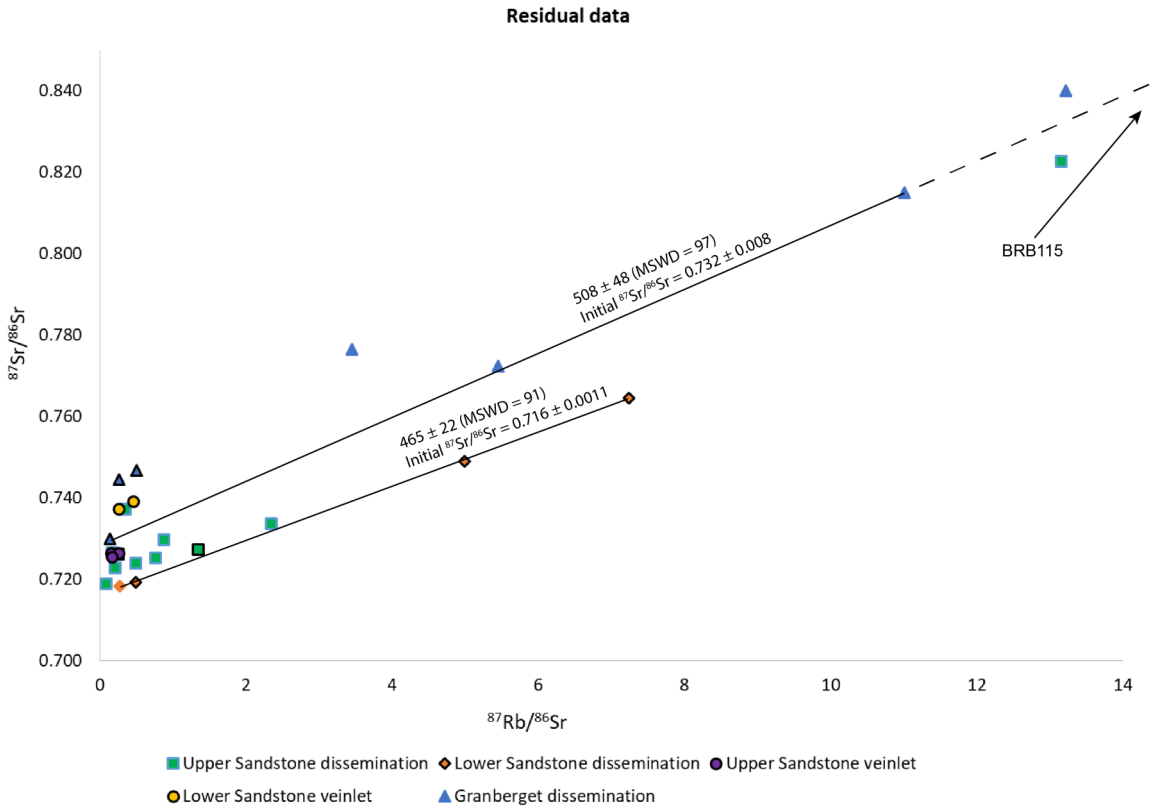

Fig. 11. Rb-Sr isotope data for compiled residual samples (this study; Saintilan et al. 2015a). Data points with black borders are from Saintilan et al. (2015a). Note the semi-parallel relationship for the Granberget samples (blue triangles). The lower regression line includes the three samples from the Lower Sandstone dissemination (orange diamonds) used by Saintilan et al. (2015a) to calculate their 467±5 Ma age; however in this diagram a fourth sample (LAQ176) is also aligned on the regression line. Data and associated error values are provided in Table. 2.

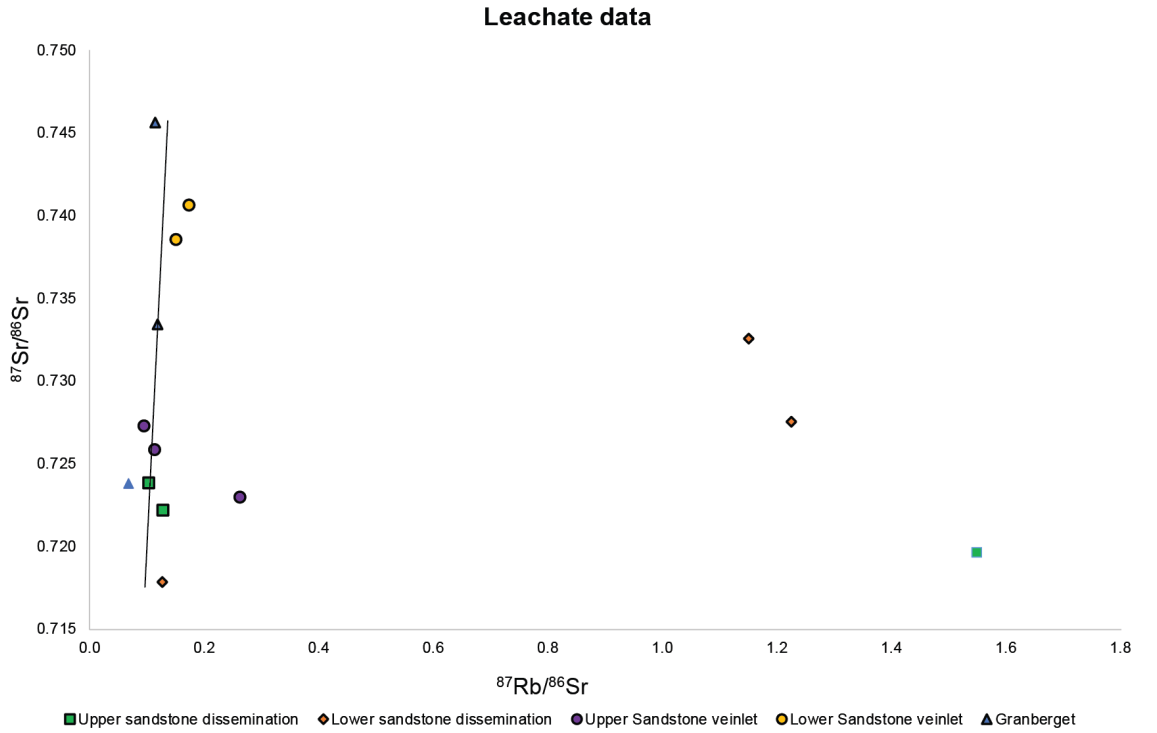

Fig. 12. Rb-Sr isotope data for leachate samples from Saintilan et al. (2015a) and this study. Note the steep linear trend that includes the majority of leachates. The markers with black borders mark data are compiled from Saintilan et al. (2015a), markers with no border are obtained in this study. Data and associated error values are provided in Table. 3.

Table 2. Rb-Sr isotope data for residual samples compiled from Saintilan et al. (2015a) and this study. Note that uncertainties given by Saintilan et al. (2015a) are absolute within-run errors, whereas standardized, relative errors (± 0.5 % in $^{87}Rb/^{86}Sr$ and ± 0.02 % in $^{87}Sr/^{86}Sr$) are used in the present study; however, the latter are recalculated to absolute errors in the table.

Ore body	$^{87}Rb/^{86}Sr$	2σ	$^{87}Sr/^{86}Sr$	2σ	Rb (ppm)	Sr (ppm)	1/Sr	Reference
Upper Sandstone dissemination								
Lv 04-09 brown	0.8803	4.40E-03	0.7297	1.46E-04	0.0799	0.2632	3.7995	This study
Lv 04-09 yellow	0.0823	4.12E-04	0.7189	1.44E-04	0.0879	3.0915	0.3235	This study
Lv 05-09 brown	13.1552	6.58E-02	0.8227	1.65E-04	2.0138	0.4479	2.2328	This study
Lv 06-09 veinlet	2.3510	1.18E-02	0.7336	1.47E-04	0.1416	0.1747	5.7228	This study
Lv 06-09 matrix brown	0.7645	3.82E-03	0.7252	1.45E-04	0.4055	1.5374	0.6505	This study
Lv 06-09 matrix yellow	0.3514	1.76E-03	0.7371	1.47E-04	0.2285	1.8863	0.5301	This study
LAQ 32	0.2073	1.04E-03	0.7229	1.45E-04	0.0872	1.2184	0.8208	This study
LAQ 158	0.4959	2.48E-03	0.7239	1.45E-04	0.1454	0.8496	1.1770	This study
LAQ 258	0.1698	8.49E-04	0.7265	1.45E-04	0.0741	1.2645	0.7908	This study
12 LAI 12 R	0.2572	3.80E-03	0.7261	2.00E-06	0.1339	1.5090	0.6627	Saintilan et al. 2015a
12 LAI 52 R	1.3503	1.93E-02	0.7272	4.00E-06	0.1677	0.3600	2.7778	Saintilan et al. 2015a
Lower Sandstone dissemination								
12 LAI 03 R	0.4949	7.10E-03	0.7192	4.00E-06	0.0973	0.5695	1.7559	Saintilan et al. 2015a
11 LAI 33 R	4.9883	7.15E-02	0.7489	1.70E-05	0.3194	0.1860	5.3763	Saintilan et al. 2015a
12 LAI 53 R	7.2453	1.17E-01	0.7645	6.00E-06	2.6007	1.0443	0.9576	Saintilan et al. 2015a
LAQ 176	0.2777	1.39E-03	0.7183	1.44E-04	0.0700	0.7300	1.3699	This study
Upper Sandstone veinlet								
12 LAI 43 R	0.1570	2.50E-03	0.7264	2.00E-06	0.1149	2.1211	0.4715	Saintilan et al. 2015a
12 LAI 44 R (1)	0.2600	3.80E-03	0.7263	2.40E-05	0.1025	1.1426	0.8752	Saintilan et al. 2015a
12 LAI 44 R (2)	0.1699	2.40E-03	0.7253	3.00E-06	0.1624	2.7714	0.3608	Saintilan et al. 2015a
Lower Sandstone veinlet								
12 LAI 14 R	0.4654	5.20E-02	0.7391	1.00E-05	0.0303	0.1892	5.2854	Saintilan et al. 2015a
12 LAI 84 R	0.2626	3.80E-03	0.7373	8.00E-06	0.0323	0.3568	2.8027	Saintilan et al. 2015a
Granberget dissemination								
BRB 50 R	0.4991	3.70E-03	0.7468	4.45E-05	0.2243	1.3051	0.7662	Saintilan et al. 2015a
BRB 56 R	0.1420	1.00E-03	0.7298	2.50E-06	0.0154	0.3144	3.1807	Saintilan et al. 2015a
BRB 58 R	0.2667	1.90E-03	0.7444	7.00E-06	0.2771	3.0170	0.3315	Saintilan et al. 2015a
BRB 74 brown	3.4482	1.72E-02	0.7765	1.55E-04	1.5402	1.3010	0.7686	This study
BRB 105 brown	13.2122	6.61E-02	0.8402	1.68E-04	2.2453	0.4981	2.0078	This study
BRB 115 (see Fig. 11 interpolation)	30.2589	1.51E-01	0.9494	1.90E-04	1.6318	0.1597	6.2610	This study
BRB 118 brown	11.0117	5.51E-02	0.8150	1.63E-04	0.2229	0.0592	16.9005	This study
BRB 119	5.4539	2.73E-02	0.7723	1.54E-04	0.1529	0.0816	12.2504	This study

Table 3. Rb-Sr isotope data for leachate samples compiled from Saintilan et al. (2015a) and this study. Note that uncertainties given by Saintilan et al. (2015a) are absolute within-run errors, whereas standardized, relative errors (± 0.5 % in $^{87}Rb/^{86}Sr$ and ± 0.02 % in $^{87}Sr/^{86}Sr$) are used in the present study; however, the latter are recalculated to absolute errors in the table.

Ore body	$^{87}Rb/^{86}Sr$	2σ	$^{87}Sr/^{86}Sr$	2σ	Reference
Upper sandstone dissemination					
Lv 04-09	1.5510	7.76E-03	0.7196	1.44E-04	This study
12 LAI 12 L	0.1025	1.50E-03	0.7238	4.00E-06	Saintilan et al. 2015a
12 LAI 52 L	0.1290	1.90E-03	0.7222	3.00E-06	Saintilan et al. 2015a
Lower sandstone dissemination					
12 LAI 03 L	0.1265	1.80E-03	0.7179	3.00E-06	Saintilan et al. 2015a
11 LAI 33 L	1.2249	2.29E-02	0.7276	2.00E-05	Saintilan et al. 2015a
12 LAI 53 L	1.1512	1.65E-02	0.7326	5.00E-06	Saintilan et al. 2015a
Upper Sandstone veinlet					
12 LAI 43 L	0.0959	1.40E-03	0.7273	6.00E-06	Saintilan et al. 2015a
12 LAI 44 L (1)	0.2635	3.80E-03	0.7230	4.00E-06	Saintilan et al. 2015a
12 LAI 44 L (2)	0.1130	1.60E-03	0.7259	3.00E-06	Saintilan et al. 2015a
Lower Sandstone veinlet					
12 LAI 14 L	0.1736	2.50E-03	0.7406	3.00E-06	Saintilan et al. 2015a
12 LAI 84 L	0.1508	2.20E-03	0.7386	3.00E-06	Saintilan et al. 2015a
Granberget					
BRB 50 L	0.1133	1.70E-03	0.7457	2.40E-05	Saintilan et al. 2015a
BRB 56 L	0.1177	1.70E-03	0.7335	4.00E-06	Saintilan et al. 2015a
BRB 115	0.0679	3.40E-04	0.7238	1.45E-04	This study

7 Discussion

The Rb-Sr isochron data obtained in this study, and others (e.g. Billstrom et al. 2012; Saintilan et al. 2015a), highlight the complexity commonly associated with sphalerite Rb-Sr isotope data from the study area, and the interpretation of potential isochrons is ambiguous. Scatter around an isochron (i.e. a straight line of data of equivalent age) can be caused by a number of processes: (1) the sphalerites crystallized during mixing of fluids with varying (initial) isotope composition; (2) the sphalerites were affected by post-mineralization perturbation leading to gain or loss of Rb and Sr, resulting in rotation or partial resetting of the isochron; (3) sphalerite crystallized over an extended time period (relative to the analytical precision); (4) contamination of the crystal lattice bound Rb and Sr from unopened micro-inclusions; (5) contamination in the laboratory environment.

Considering the last two of these hypothetical explanations, a small effect cannot be totally ruled out. However, data are blank-corrected in order to remove the effect of contamination of samples in the chemistry laboratory and since the samples were thoroughly grinded (allowing the content of fluid inclusions to be liberated), it is assumed that their effect on the Rb-Sr sphalerite system, defined by residual samples, can be neglected. When considering possible age differences among samples, these may exist as specimens represent different sampling locations and textural settings. On the other hand, the observation that a scatter is also seen for samples representing a single ore type hosted within a specific ore horizon (e.g. disseminated-style samples from within the Upper sandstone) is strongly suggesting that age differences is not the main cause for the overall scatter.

Excluding the aforementioned causes for the apparent diachroneity within and between sample sets, post-ore disturbances and heterogeneity of initial Sr isotope ratios in the ore fluids remain as plausible explanations. The independent age constraints that are available at Laisvall are limiting ore formation to between ca. 540 and 425 Ma. The upper limit is defined by the observation that mineralization at Laisvall to some extent also affected Cambrian units within the Ediacaran-Cambrian package of ore-bearing sandstones. The lower age limit of the Laisvall mineralization is constrained by deformation during the culmination of the Caledonian orogeny around 425 Ma. Given these age constraints, the linear arrays with slopes corresponding to an age in the approximate 540–425 Ma interval warrant further consideration. Basically, two ideas will be contrasted below; the effect of a post-crystallization disturbance as discussed by Saintilan et al. (2015a) versus the effect of syn-ore fluid heterogeneities in the initial Sr isotope composition (Billström et al., in prep.)

7.1 The possibility of a post-mineralization disturbance affecting the Rb-Sr system

Saintilan et al. (2015a) argue for a post-mineralization disturbance of the Rb-Sr isotope system by Sr-rich fluids in the Upper Sandstone at Laisvall. These authors suggest that samples within the Lower sandstone member were not affected by post-ore disturbance and they interpret a three-point isochron of 467 ± 5 Ma (MSWD = 1.4) Ma to date the age of mineralization of the Laisvall ores. Yet, they note that samples from the Upper sandstone member were partly disturbed. One disseminated residue sample from the Upper sandstone (12LAI12 R), along with leachate samples, fits a steep linear array of $^{87}Rb/^{86}Sr$ vs $^{87}Sr/^{86}Sr$ isotope data (Fig. 5A in Saintilan et al. 2015a). The slope of this array yields an impossibly old age, and the array was considered to be a mixing trend. The steep linear trend was interpreted as a result from Sr-gain through infiltration of radiogenic Sr-rich fluids, which are inferred to have generated the mineralized veinlets through remobilization (Saintilan et al. 2015a). LA-ICPMS data of element concentrations, suggests that Upper Sandstone samples have been disturbed, as indicated by the scatter produced in [Sr] vs. [Rb] diagram (Fig. 7A and 7B in Saintilan et al. 2015a), whereas Lower Sandstone samples plot relatively linear indicating limited or no disturbance (Saintilan et al. 2015a). Other factors supporting a local post-ore disturbance is the occasionally tectonically disrupted Upper Sandstone and its proximity to the lowermost Caledonian nappe thrust plane and the presence of cross-cutting steeply dipping galena-sphalerite-calcite veinlets. The mineralized cross-cutting joints might have formed during remobilization which took place after formation of the disseminated sandstone ores, as proposed by Saintilan et al. (2015a). Similarly, the Granberget ore body is disrupted by sub-vertical faults, cut by mineralized veins with an overall overprinting of low-angle thrusts (Saintilan et al. 2015a) and thought to have been affected by late Sr-bearing fluids.

In summary, Saintilan et al. (2015a) consider that the Rb-Sr sphalerite system in the Lower sandstone at Laisvall closed at 467 Ma, whereas this took place later (probably around 425–400 Ma) for veinlet samples and samples from the Upper sandstone that were affected by a late Sr gain.

7.2 The possibility of syn-ore processes creating heterogenities in Sr initial isotope values

Instead of a secondary gain as the mechanism behind the Rb-Sr scatter, it is possible that it is due to heterogeneities in initial Sr isotope values. Focusing on the Laisvall-type of ores, the latter hypothesis would assume that the Rb-Sr sphalerite system in e.g. the disseminated Laisvall ore bodies closed at a common time at some point within the 540–425 Ma interval. A reasonably good constraint on the Sr isotope values valid at the time of Rb-Sr system closure is obtained by focusing on samples having low Rb/Sr ratios. Such samples have not been affected to a large extent by ^{87}Rb decay (producing radiogenic ^{87}Sr and thereby changing the Sr isotope ratio) and are as such reflectors of the situation at the time designating the closure of the Rb-Sr system. Calculations have been carried out for samples with a Rb/Sr ratio of less than 1.0; this is an arbitrary value, but the exact number for this parameter is not crucial for this discussion. Any calculation of an initial Sr value requires that the measured Sr isotope composition for a single sample is back-

calculated to the value valid at the time of anticipated starting time. However, it cannot be determined a priori when the Rb-Sr systems closed. For this discussion, it is notable that the age correction is insensitive to any age in the 540–425 Ma interval. This is due to the relatively minor differences in slope values for different ages within the discussed age span (slope value for 540 and 425 Ma is 0.00753 and 0.00592, respectively) and the associated small effect on calculated $^{87}Sr/^{86}Sr_{initial}$ isotope values. Thus, if a crude, intermediate ore forming age of 500 Ma is used for all samples low in Rb/Sr from Granberget and Laisvall, it can be argued that disseminated samples from Laisvall had $^{87}Sr/^{86}Sr$ isotope values between ca 0.716 and 0.725, whereas Granberget samples may define a dual mode with values close to ca 0.732 and 0.742, respectively. The observation that the initial Sr-isotope values are significantly different implies that isotopically different ore fluids must be inferred, and also that the observed tendency for straight-line arrays can only be explained if a number of specimens share the same initial Sr isotope composition.

Several circumstances provide support for the idea that ore fluids had variable Sr isotope compositions. First, fluid inclusion data that is based on homogenization temperatures and salinity from Laisvall and Granberget show no signs of being secondary or disturbed by Caledonian tectonics. Second, sphalerite crystals display undisturbed, symmetric growth zoning, yielding support for a low-stress growth environment (Rickard et al. 1979). These observations, in conjunction with the absence of annealing and deformation lamellas in sphalerite, suggest that sphalerite has not been significantly altered or recrystallized. Studies of healed fractures in quartz grains imply that these fractures formed prior to the infilling of the interstitial volumes and the mineralization of the sandstones at Laisvall (Lindblom 1986). The thrusts and faults cross-cutting the mineralization are related to clay layers in the sandstones, leaving most of the interior of the sandstone blocks unaffected from deformation (Lindblom 1986). Moreover, the tectonic disturbance caused by the lowermost nappe has been considered to be insignificant ca. 20 m below the thrust plane, which corresponds to a stratigraphic position well above the Upper sandstone member. Finally, the metamorphic grade was below the temperature for ore formation as shown in results from illite crystallinity (Rickard et al. 1979).

The main point made by these observations is that only minor post-crystallization effects on minerals and their isotope systems appear to have occurred, and that all significant ore features developed at a syn-ore stage. Therefore, there is no obvious reason to invoke Rb or Sr mobilization as a cause for the data scatter. On the contrary, the Rb-Sr isotope data scatter is consistent with heterogeneities in the initial Sr isotopic compositions of syn-depositional ore-bearing fluids, and provides a better explanation given independent geological evidence.

7.3 Fluid mixing and ore-forming processes

Irrespective of whether post-mineralization disturbance or syn-ore heterogeneities in initial Sr isotope ratios are invoked as an explanation for the lack of simple isochrones, the data share one parameter; Rb-Sr mixing or perturbation must have taken place during or after mineralization. Certainly, the model assuming variable initial Sr isotope compositions is consistent with the presence of isotopically different ore fluids. Their presence is supported by e.g. color zoning and a variable metal distributions as noted at Laisvall, and it has been proposed by authors (Rickard et al. 1979; Lindblom 1986) that several, discrete ore fluids have formed the Laisvall ore. Thus, it seems highly unlikely that a single ore-fluid is responsible for the large $^{87}Sr/^{86}Sr$ signature contrast typifying disseminated samples from Laisvall and Granberget, ranging from common ($^{87}Sr/^{86}Sr$ ca. 0.718) to highly radiogenic ($^{87}Sr/^{86}Sr$ ca. 0.949) isotope values on a sampling scale.

A similar type, and magnitude, of Rb-Sr isotope data scatter as seen for the disseminated ores has also been observed for the Zn-Pb vein ores in the Lycksele-Storuman region (Billstrom et al. 2012). These authors discussed different mixing scenarios that could explain the observed scatter and anticipated the presence of at least two types of fluids; 1) an isotopically homogenous, un-radiogenic fluid referred to as the 'cool fluid'. This fluid mainly comprises Sr from seawater and less radiogenic meteoric water, and 2) a hot, metal-rich fluid originating from the basement with a more radiogenic Sr-isotope composition, referred to as a 'hot fluid'. In one proposed scenario, a distinction was made between two types of sphalerite; one population formed from the isotopically homogeneous cool fluid giving rise to a linear Rb-Sr array, and one scattered population that precipitated as a result of on-site mixing between the cool fluid and the radiogenic hot fluid. Similar arguments could apply to the Laisvall and Granberget ores, and the wide range in homogenization temperatures and salinity of the fluid inclusions from Laisvall provides further evidence for the ore solution(s) being the result of mixing of two, or more, fluids. The higher calculated $^{87}Sr/^{86}Sr$ isotope values of 0.732 and 0.742 for Granberget compared to values between 0.716 and 0.725 for Laisvall, would suggest that the fluids forming the Granberget ore had a larger influx of the radiogenic, hot fluid component. Interestingly, the lower end of the isotope compositional spectrum of the ore-forming fluids at Laisvall is close to the value (ca. 0.716) representing the samples that were used to calculate the ca. 530 Ma isochron age for the vein hosted Pb-Zn ore type (Billstrom et al. 2012).

There are tendencies for residual sphalerite samples to plot along linear arrays and, principally, any straight line can be interpreted as either a mixing line or an isochron. The former explanation assumes physical mixing of two components of different Sr concentration and Sr isotope ratios, whereas an isochron is based on the assumption that samples of the same age, and sharing identical initial Sr isotope compositions would plot along a straight line. A commonly used approach to distinguish between mixing and isochrons is to plot the measured Sr-isotope composition against the reciprocal strontium concentration (Fig. 13). Data that define a straight line suggests the presence of mixing, while there is no prerequisite reason for isochronous data to plot along systematic

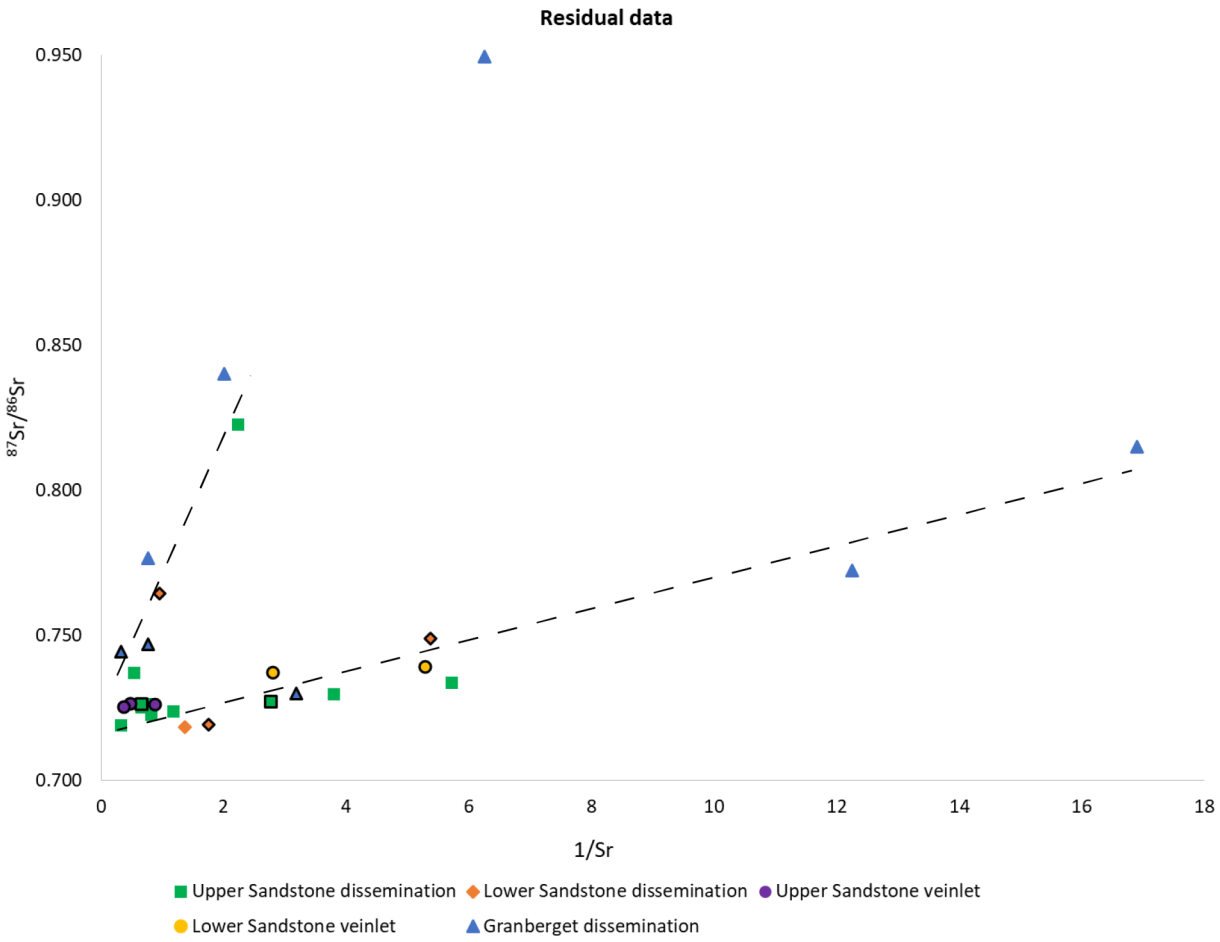

Fig. 13. Residue Rb-Sr isotope data plotted vs. 1/Sr (ppm). Data points compiled from the literature are marked with black borders while remaining points are obtained in this study. The two linear trends are shown with dashed lines.

trends. This approach is particularly useful for modern samples that contain no radiogenic ingrowth of daughter isotopes. However, a complexity with the present data set is that mixing has been demonstrated to have affected the sample data (most likely it occurred in connection with syn-ore processes or a few tenths of million years after the crystallization of sphalerite) and moreover, the significant levels of Rb in in residual samples imply that radiogenic ^{87}Sr has been produced. Here, ancient mixing of sources with contrasting Sr-isotope compositions as well as variable radiogenic ingrowth as a function of Rb/Sr controls the data in Fig. 13, leading to a rather complex data pattern. Samples that have been previously suggested to be isochronous do not form a straight line in the reciprocal Sr diagram (Fig. 13), implying that they might indeed have age significance. On the other hand, most samples in Fig. 13 define two linear arrays and a possible explanation is that these arrays constitute separate binary mixing trends involving three different source end-members (Billström et al., in prep.).

Saintilan et al. (2015a) presented a scenario where the ore fluids were a mixture of highly radiogenic $^{87}Sr/^{86}Sr$ leached from permeable Proterozoic basement rocks and a sedimentary source with a less radiogenic $^{87}Sr/^{86}Sr$ composition. The fluids were hypothesized to originate during the development of an early Caledonian foreland basin, which would have generated a mixture of basement-leached metal rich brines with hydrocarbons and thermochemical reduced sulfur originating from organic rich shales (Rickard et al. 1975; Saintilan et al. 2015a). Basically, the principal development of ore-forming fluids, as outlined by Saintilan et al. (2015a) from their studies on the Laisvall ore, is a realistic scenario and it is not dependent on which model that is preferred to explain Rb-Sr isotope data scatter. What may be emphasized is that it seems likely that ore formation at Laisvall did not occur in a single static system; it probably had the nature of a dynamic system in which different, single ore fluids followed different paths and equilibrated with slightly different types of host rocks.

7.4 Age estimates and possible genetic links between ores of different types

Two mechanisms for the scattered Rb-Sr isotope data have been discussed in this work. Saintilan et al. (2015a) put forward an idea of a post-addition gain of Sr. There is no firm evidence emerging in the present work that reject this hypothesis, but the data presented here show that there is also a possibility that the scatter may be due to intrinsic, isotopic properties of ore-bearing fluids. Following the latter hypothesis, the measured $^{87}Sr/^{86}Sr$ isotope compositions is a function of two processes; (1) the presence of several ore pulses with variable Sr isotope signatures, and (2) the in-situ

growth of ^{87}Sr due to the effect of ^{87}Rb decay. Despite that the former process ultimately led to a complicated Rb-Sr data scatter, it appears that there are certain subgroups of samples with high $^{87}Rb/^{86}Sr$-ratio that tend to define straight-line relationships and, as discussed above, such arrays are likely to have an age significance. The immediate question to be asked is when ore formation occurred for different ore types. Below follows a brief discussion about the timing of ore formation leading to the A) main, strata-bound Pb-Zn disseminated ores (principal ore type at Laisvall and Granberget), the B) Pb-Zn veinlets overprinting the disseminated ores, and the C) breccia-hosted Zn-Pb vein-type in e.g. the Lycksele-Storuman area.

Temporal constraints that can put the Pb-Zn mineralization events into a geological framework are poor. As discussed earlier, field evidence infer disseminated mineralization to be restricted to an approximate 540-425 Ma interval. Rb-Sr isotope sphalerite data of disseminated Laisvall samples (Saintilan et al. 2015a; this study) do not provide any unequivocal evidence, and the significance of the precise 467 ± 5 Ma isochron offered for the Laisvall mineralization (Saintilan et al. 2015a) can be questioned as it relies on three data points (Billström et al. in prep.). There is a tendency for certain samples from Granberget to plot on a linear array (this study), which could be interpreted as a crude 500 Ma isochron age, but no firm conclusions can be made. Similarly, Rb-Sr sphalerite data from deposits in the Lycksele-Storuman area (Billstrom et al. 2012), tentatively indicating a ca. 530 Ma age, are not particularly robust. There are also Ar-Ar data for late rim over-growths on K-feldspars sampled in Laisvall sandstones which argue for two hydrothermal events at ca 567–528 and 453–403 Ma, respectively (Sherlock et al. 2005). These age intervals are interpreted as two separate periods with the older age(s) being a result of burial diagenesis and the younger age(s) being a result of tectonically induced fluid flow caused by the orogenic collapse of the Caledonides and development of intra-orogenic basins (Sherlock et al. 2005; Saintilan et al. 2015a). It appears possible that either or both of these periods correspond with fluid flow events connected to mineralizing processes.

On the other hand, mineralogy, fluid inclusion data and textural relationships may help to set up probable models for ore formation. Saintilan et al. (2016b) proposed that, based on isotope data ($\delta^{13}C$, $\delta^{18}O$ and $\delta^{34}S$) from studies on calcite-fluorite-sulphide vein deposits along the erosional Caledonian front at Åkerlandet and in the granitic basement at Laisvall, the gangue minerals calcite and fluorite were precipitated from mixing of an evolved and basement-interacted, near-neutral (pH 5–6), metal-poor, reduced fluid and H_2S-rich fluids originating from organic rich layers such as the Alum shale formation. Comparable fluids were likely involved in the disseminated style of ore formation, and it is also possible that the veinlets cross-cutting the disseminated sandstone ores formed more or less simultaneously with the disseminated ore. The latter scenario is supported by results from homogenization temperatures and melting temperatures for sphalerite in the mineralized joints and in the disseminated ore, indicating an identical bulk composition and temperature for the fluids precipitating the disseminated ores and different veinlet mineralization (Rickard et al. 1979). Another important observation is that breccia vein deposits at Åkerlandet, Järvsand and in the Lycksele-Storuman district share several characteristics in mineralogy and fluid inclusions with the Laisvall disseminated ore. This is indicating common, regionally driven processes, which raises the option that breccia- and disseminated ore types actually formed by synchronous processes. That is, there remains a possibility that regional-scale hydrothermal cells affected large areas, and that metal-bearing fluids during ascent deposited sulphide ore in veins in the basement as well as filled up pores in sandstones.

The paleogeographic setting at e.g. Åkerlandet and Laisvall was similar during the 540–425 Ma interval, i.e. a package of autochtonous sedimentary rocks overlaid an old Proterozoic basement which is consistent with a coeval deposition of different ore types. This is in opposition to the idea put forward by Saintilan et al. (2015a) who interpreted the basement hosted calcite-fluorite-sulphide veins to post-date the formation of the Pb-Zn mineralized sandstones at Laisvall and suggested that these veins have been active at multiple intervals and possibly acting as a conveying system for the metal-rich fluids precipitating the Laisvall sandstone hosted Pb-Zn ore. The uncertain temporal relationship between vein deposits and disseminated ores is reinforced by the way Rb-Sr sphalerite isotope data for these ore types plot in diagrams. Saintilan et al. (2015a) did not conclude whether or not the vein deposits actually formed more or less simultaneously with the disseminated ores at ca 467 Ma, or if their formation preceded the event leading to disseminated ores by ca 70 million years. Determining a precise and accurate age for mineralization is fundamentally important as it has bearing on our understanding of the mineralizing processes. For instance, if the age of mineralization is ca. 540 Ma, it would be related to far-field effects in response to tectonic activity during the Timian orogeny along the north-eastern margin of Baltica, whereas a younger 467 Ma event would be consistent with early Caledonian compressive tectonic activity (Saintilan et al. 2015a).

8 Conclusion

The nature of the Rb-Sr sphalerite isotope data presented in this study is complex and any interpretation is ambiguous. Two main hypotheses have been discussed for the cause of the observed scatter; (1) late Sr-gain caused by post-mineralization disturbance (Saintilan et al. 2015a), and (2) mixing of fluids with heterogeneous $^{87}Sr/^{86}Sr$ isotope values and ^{87}Sr growth due to ^{87}Rb in-situ decay (Billström et al in prep.). Both models assume mixing to have occurred. However, the data presented here is consistent with varying $^{87}Sr/^{86}Sr_{initial}$ isotope values that can be constrained when back-calculating from measured Sr isotope values. Even though no precise age for the ore-forming processes at Laisvall and Granberget can be presented here, our data support the model of a regional-scale hydrothermal fluid flow, driven by far-field orogenic tectonics (either by older Timian or by younger Caledonian tectonics). Moreover, the highly variable $^{87}Sr/^{86}Sr_{initial}$ isotope data obtained in this study further

support a model of syn-ore formation mixing of fluids with varying Sr-isotope compositions. It is quite likely that these processes formed several types of Pb-Zn deposits at different locations in the vicinity of the Caledonides during a relatively short time interval. The duration of a large-sized hydrothermal ore is normally in the range of hundreds of thousands of years to a few million years, and may involve several short-lived pulses. If hypothetically, in the current context, one major hydrothermal event led to the deposition of different ore types distributed over a large geographical area it is believed that the life-time of such an event is within the analytical uncertainty of any age based on radiogenic decay schemes.

9 Acknowledgements

First and foremost I wish to thank my supervisors, Anders Scherstén and Kjell Billström. Kjell for introducing me to the Laisvall project, supervision through the laboratory work and providing an essential source of information as well as editorial support. I wish to thank Anders for mentoring me through the process of the thesis work and assisting with all kinds of difficulties. Last but not least, I want to thank my fellow thesis workers on the 5th floor Jon, Johan, Josefin, Robin, Anders, Viktor, Tawo, Joaen, Markus and Fredrika. You all made the days so much more enjoyable.

10 References

Attendorn, H.-G., 1997: *Radioactive and stable isotope geology*. London. Chapman & Hall, 522 pp.

Bastin, E. S., 1939: Theories of formation of ore deposits. *Scientific American 49*, 538–547.

Billstrom, K., Broman, C., Schneider, J., Pratt, W. & Skogsmo, G., 2012: Zn-Pb Ores of Mississippi Valley type in the Lycksele-Storuman District, Northern Sweden: A Possible Rift-Related Cambrian Mineralisation Event. *Minerals 2*, 169–207.

Billström, K., Broman, C., Larsson, A., Karlsson, A., Hogmalm, J., Årebäck, H. (in preparation): Further constraints on the age and fluid sources in sandstone-hosted Pb-Zn mineralisation in the Swedish Caledonides.

Bjørlykke, A. & Sangster, D. F., 1981: An overview of sandstone lead deposits and their relation to red-bed copper and carbonate-hosted lead-zinc deposits. *Economic Geology 75th Anniversary Volume*, 179–213.

Brannon, J. C., Podosek, F. A. & Mclimans, R. K., 1992: Alleghenian age of the Upper Mississippi Valley zinc-lead deposit determined by Rb-Sr dating of sphalerite. *Nature 356*, 509–511.

Casanova, V., 2010: Geological and geophysical characteristics of the Pb-Zn sandstone-hosted autochthonous Laisvall deposit in the perspective of regional exploration at the Swedish Caledonian Front. *Luleå University of Technology*. 32 pp.

Chi, G., Qing, H., Xue, C. & Zeng, R. 2005: An overpressured fluid system associated with the giant sandstone-hosted Jinding Zn-Pb deposit, western Yunnan, China. *In* J. Mao & F. P. Bierlein (eds.): *Mineral Deposit Research: Meeting the Global Challenge: Proceedings of the Eighth Biennial SGA Meeting Beijing, China, 18–21 August 2005*, 93–96.

Christensen, J. N., Halliday, A. N., Leigh, K. E., Randell, R. N. & Kesler, S. E., 1995: Direct dating of sulfides by Rb-Sr: A critical test using the polaris Mississippi Valley-type Zn-Pb deposit. *Geochimica Et Cosmochimica Acta 59*, 5191–5197.

Christofferson, H. C., Wallin, B., Selkman, S. & Rickard, D. T., 1979: Mineralization controls in the sandstone lead-zinc deposits at Vassbo, Sweden. *Economic Geology 74*, 1239–1249.

Dallmeyer, R. D. & Gee, D. G., 1986: $^{40}Ar/^{39}Ar$ mineral dates from retrogressed eclogites within the Baltoscandian miogeocline: Implications for a polyphase Caledonian orogenic evolution. *Geological Society of America Bulletin 97*, 26–34.

Dickin, A. P., 2005: *Radiogenic isotope geology*. Cambridge. Cambridge University Press, 492 pp.

Faure, G., 1986: *Principles of isotope geology*. New York. Wiley, cop., 589 pp.

Gee, D. G., 1975: A tectonic model for the central part of the Scandinavian Caledonides. *American Journal of Science v. 275A*, p. 468–515.

Gee, D. G., Juhlin, C., Pascal, C. & Robinson, P., 2010: Collisional Orogeny in the Scandinavian Caledonides (COSC). *Geologiska Föreningen i Stockholm Förhandlingar 132*, 29–44.

Grip, E., 1954: Blymalmen vid Laisvall, dess geologi och en jämförelse med några utländska förekomster. *Geologiska Föreningen i Stockholm Förhandlingar 76*, 357–380.

Johansson, A. & Rickard, D., 1984: Isotopic compositions of phanerozoic ore leads from the Swedish segment of the Fennoscandian shield. *Mineralium Deposita 19*, 249–255.

Kendrick, M. A., Burgess, R., Harrison, D. & Bjorlykke, A., 2005: Noble gas and halogen evidence for the origin of Scandinavian sandstone-hosted Pb-Zn deposits. *Geochimica Et Cosmochimica Acta 69*, 109–129.

Leach, D. L., Bradley, D. C., Huston, D., Pisarevsky, S. A., Taylor, R. D. & Gardoll, S. J., 2010: Sediment-Hosted Lead-Zinc Deposits in Earth History. *Economic Geology 105*, 593–625.

Leach, D. L., Dwight, B., Lewchuk, M. T., Symons, D. T. A., De Marsily, G. & Brannon, J., 2001: Mississippi Valley-type lead-zinc deposits through geological time: implications from recent age-dating research. *Mineralium Deposita 36*, 711–740.

Leach, D. L. & Sangster, D. F., 1993: Mississippi Valley-type lead-zinc deposits. *Geological Association of Canada Special Paper 40*, p. 289–314.

Leach, D. L., Sangster, D. F., Kelley, K. D., Large Ross, R., Garven, G. & Allen, C. R., 2005: Sediment-hosted Pb-Zn Deposits: a global perspective. *Economic Geology 100*, 561–608.

Leach, D. L. & Taylor, R. D., 2009: Mississippi Valley-type lead-zinc deposit model. *U.S. Geological Survey Open-File Report 2009-1213*, 5 p.

Lindblom, S., 1986: Textural and fluid inclusion evidence for ore deposition in the Pb-Zn deposit at Laisvall, Sweden. *Economic Geology 81*, 46–64.

Ljungner, E., 1950: Urbergsytans form vid fjällranden. *Geologiska Föreningens i Stockholm Förhandlingar 72*, 269–300.

Ludvig, K. R., 2001: User's manual for Isoplot/Ex, rev. 2.49, A geochronological toolkit for Microsoft Excel. *Berkeley Geochronology Center Special Publication 1a, Berkeley CA*, 59 p.

Moczydlowska, M., Jensen, S., Ebbestad, J. O. R., Budd, G. E. & Marti-Mus, M., 2001: Biochronology of the autochthonous Lower Cambrian in the Laisvall-Storuman area, Swedish Caledonides. *Geological Magazine 138*, 435–453.

Nakai, S., Halliday, A. N., Kesler, S. E., Jones, H. D., Kyle, J. R. & Lane, T. E., 1993: Rb-Sr dating of sphalerites from Mississippi Valley-type (MVT) ore-deposits. *Geochimica Et Cosmochimica Acta 57*, 417–427.

Nakai, S. I., Halliday, A. N., Kesler, S. E. & Jones, H. D., 1990: Rb-Sr dating of sphalerites from Tennessee and the genesis of Mississippi Valley type ore deposits. *Nature 346*, 354–357.

Nielsen, A. T. & Schovsbo, N. H., 2011: The Lower Cambrian of Scandinavia: Depositional environment, sequence stratigraphy and palaeogeography. *Earth-Science Reviews 107*, 207–310.

Paradis, S., Hannigan, P. & Dewing, K., 2007: Mississippi Valley-type lead-zinc deposits. *Geological Association of Canada, Mineral Deposits Division, St. John's, NL, Canada 5*, 185–204.

Pettke, T. & Diamond, L. W., 1996: Rb-Sr dating of sphalerite based on fluid inclusion-host mineral isochrons: A clarification of why it works. *Economic Geology and the Bulletin of the Society of Economic Geologists 91*, 951–956.

Rickard, D. T., Willden, M., Marde, Y. & Ryhage, R., 1975: Hydrocarbons associated with lead-zinc ores at Laisvall, Sweden. *Nature 255*, 131–133.

Rickard, D. T., Willden, M. Y., Marinder, N. E. & Donnelly, T. H., 1979: Studies on the genesis of the Laisvall sandstone lead-zinc deposit, Sweden. *Economic Geology 74*, 1255–1285.

Roberts, D. & Gee, D. G., 1985: An introduction to the structure of the Scandinavian Caledonides, *in* Gee, D.G., and Sturt, B.A., eds., The Caledonide orogen—Scandinavia and related areas. *Chichester, Wiley*, p. 55−68.

Roedder, E., 1968: Environment of deposition of the disseminated lead ores at Laisvall, Sweden, as indicated by fluid inclusions. *International Geological Congress XXIII, 7*, 389–401.

Romer, R. L., 1992: Sandstone-hosted lead-zinc mineral deposits and their relation to the tectonic mobilization of the Baltic shield during the Caledonian orogeny - a reinterpretation. *Mineralogy and Petrology 47*, 67–85.

Saintilan, N. J., 2015: Key controls, age, source of metals, and role of organic matter on the origin of Laisvall-type Pb-Zn deposits and their relationship to calcite-fluorite-Zn ± Pb sulfide vein-type mineralization in Baltica Basement (Sweden). *University of Genève, PhD Thesis*.

Saintilan, N. J., Schneider, J., Stephens, M. B., Chiaradia, M., Kouzmanov, K., Walle, M. & Fontbote, L., 2015a: A Middle Ordovician Age for the Laisvall Sandstone-Hosted Pb-Zn Deposit, Sweden: A Response to Early Caledonian Orogenic Activity. *Economic Geology 110*, 1779–1801.

Saintilan, N. J., Spangenberg, J. E., Samankassou, E., Kouzmanov, K., Chiaradia, M., Stephens, M. B. & Fontbote, L., 2016a: A refined genetic model for the Laisvall and Vassbo Mississippi Valley-type sandstone-hosted deposits, Sweden: constraints from paragenetic studies, organic geochemistry, and S, C, N, and Sr isotope data. *Mineralium Deposita 51*, 639–664.

Saintilan, N. J., Stephens, M. B., Lundstam, E. & Fontbote, L., 2015b: Control of Reactivated Proterozoic Basement Structures on Sandstone-Hosted Pb-Zn Deposits along the Caledonian Front, Sweden: Evidence from Airborne Magnetic Data, Structural Analysis, and Ore-Grade Modeling. *Economic Geology 110*, 91–117.

Saintilan, N. J., Stephens, M. B., Spikings, R., Schneider, J., Chiaradia, M., Spangenberg, J. E., Ulianov, A. & Fontboté, L., 2016b: Polyphase vein mineralization in the Fennoscandian Shield at Åkerlandet, Järvsand, and Laisvall along the erosional front of the Caledonian orogen, Sweden. *Mineralium Deposita*, 1–22.

Schneider, J., Melcher, F. & Brauns, M., 2007: Concordant ages for the giant Kipushi base metal deposit (DR Congo) from direct Rb-Sr and Re-Os dating of sulfides. *Mineralium Deposita 42*, 791–797.

Selby, D., Creaser, R. A., Dewing, K. & Fowler, M., 2005: Evaluation of bitumen as a ^{187}Re-^{187}Os geochronometer for hydrocarbon maturation and migration: A test case from the Polaris MVT deposit, Canada. *Earth and Planetary Science Letters 235*, 1–15.

Sherlock, S. C., Lucks, T., Kelley, S. P. & Barnicoat, A., 2005: A high resolution record of multiple diagenetic events: Ultraviolet laser microprobe Ar/Ar analysis of zoned K-feldspar overgrowths. *Earth and Planetary Science Letters 238*, 329–341.

Steiger, R. H. & Jäger, E., 1977: Subcommission on geochronology: Convention on the use of decay constants in geo- and cosmochronology. *Earth and Planetary Science Letters 36*, 359–362.

Stephens, M. B., 1988: The Scandinavian Caledonides: a complexity of collisions. *Geology Today 4*, 20–26.

Stephens, M. B., Wahlgren, C.-H. & Weihed, P., 1994: Geological Map of Sweden, Scale 1:3 Million Ba52. *Geological Survey of Sweden: Uppsala, Sweden*.

Villa, I. M., De Bievre, P., Holden, N. E. & Renne, P. R., 2015: IUPAC-IUGS recommendation on the half life of Rb-87. *Geochimica Et Cosmochimica Acta 164*, 382-385.

Willdén, M. Y., 1980: *Paleoenvironment of the Autochthonous Sedimentary Rock Sequence at Laisvall, Swedish Caledonides*. Distributor, Almqvist & Wiksell.

Xue, C. J., Zeng, R., Liu, S. W., Chi, G. X., Qing, H. R., Chen, Y. C., Yang, J. M. & Wang, D. H., 2007: Geologic, fluid inclusion and isotopic characteristics of the Jinding Zn-Pb deposit, western Yunnan, South China: A review. *Ore Geology Reviews 31*, 337–359.

11 Appendix

Laisvall NADOK Lv 04-09

Thin section description: Mineralization is composed of fine grained honey-yellow sphalerite occupying the pore-spaces between quartz grains. Distinguishing for this sample is that the sphalerite is honey-yellow to greenish. The sandstone is well-sorted compared to the Granberget breccia sandstones. The sphalerite distribution appear to be disseminated to a higher degree.
Main mineralogy: Quartz, sphalerite, galena
Grain size: Medium grained.
Grain shapes: Rounded to sub-rounded quartz grains compose the matrix. Honey-yellow sphalerite is intergrown in interstitial spaces.
Sorting: Well-sorted
Intergrain relationships: Grain supported. Quartz compose matrix. Mainly sphalerite is occupying pore-spaces.
Textural maturity: Mature to supermature.

Laisvall 05-09 Nadok ort 807 Upper sandstone

Thin section description: Rich on fine grained dark, brownish sphalerite and local galena mineralizations. This Laisvall sample display sphalerite with a darker tint compared to Laisvall 04-09 sample. Still, the sphalerite is more disseminated compared to Granberget samples. Additionally, the Laisvall samples have more rounded quartz grains, are well-sorted and texturally mature. Galena content seem to be relatively low compared to Granberget breccia-type of mineralization.
Main mineralogy: Quartz, sphalerite, ± galena
Grain size: Fine grained.
Grain shapes: Sub-rounded quartz grains compose the matrix.
Sorting: Well-sorted
Intergrain relationships: Grain supported. Quartz compose matrix. Sphalerite ± local galena is occupying pore-spaces.
Textural maturity: Mature.

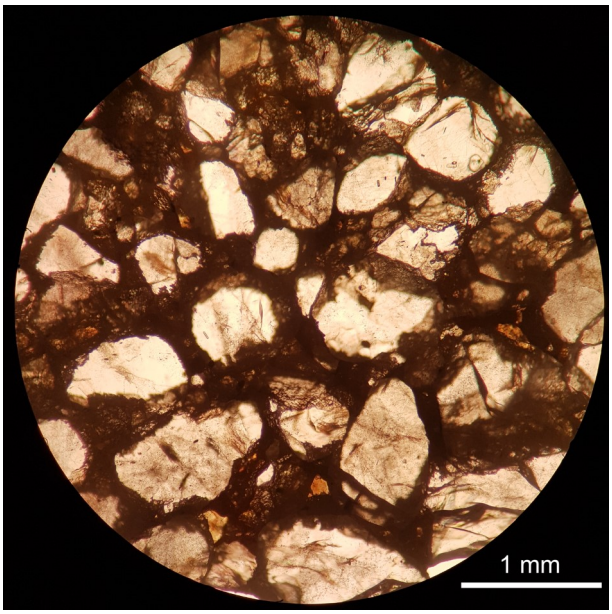

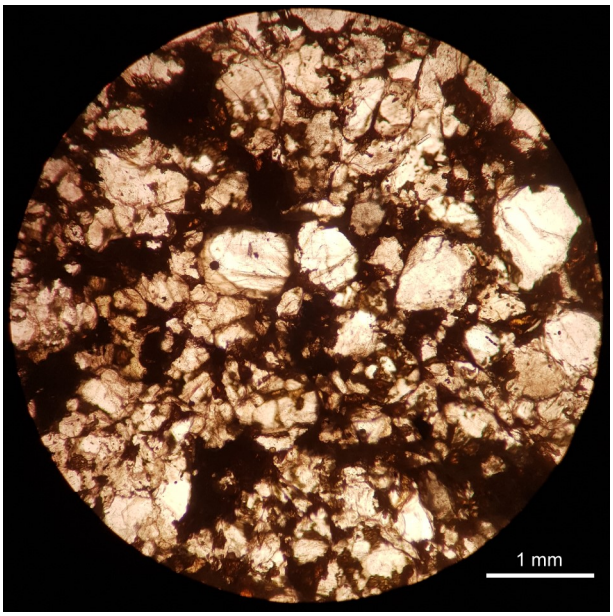

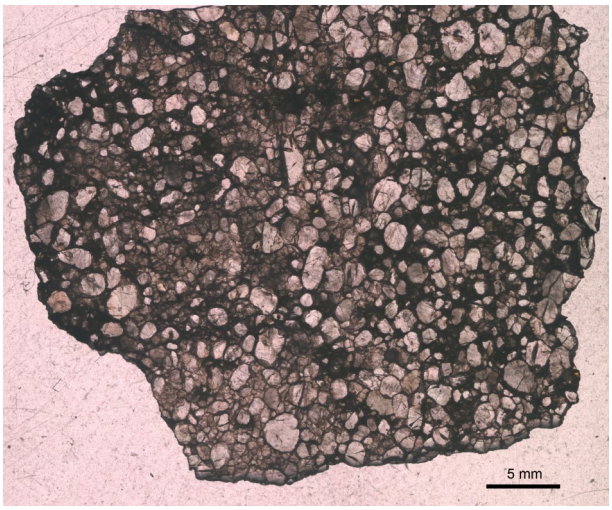

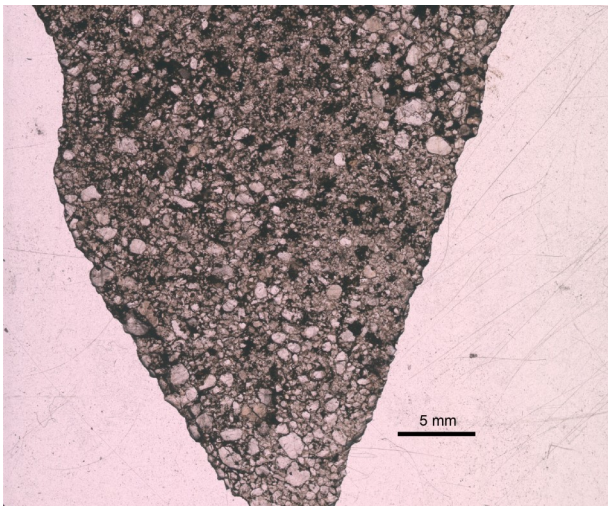

Laisvall LAI Bh1020

Thin section description: Rich on dark sphalerite and galena. Similar to the other Laisvall sample, the sandstone is relatively well-sorted and the ore is coating the quartz grains.
Main mineralogy: Quartz, sphalerite, ± galena
Grain size: Medium to coarse grained.
Grain shapes: Sub-rounded quartz grains compose the matrix. Sulphides are cementing the rock.
Sorting: Moderately sorted.
Intergrain relationships: Grain supported. Quartz compose matrix. Galena ± sphalerite is occupying pore-spaces.
Textural maturity: Submature to mature.

Laisvall LAI Bh 1243 43.25 – 43.48 m

Thin section description: Sample is richly mineralized on brownish sphalerite and locally accessory shiny greyish galena. Sorting is less pronounced compared to Lv 04-09 and Lv 05-09. Galena mineralizations are only local and clustered. Sphalerite occur as cement network in the interstitial spaces throughout the sample.
Main mineralogy: Quartz, sphalerite, galena
Grain size: Medium to coarse grained.
Grain shapes: Sub-rounded to rounded quartz clasts are the dominating phase. Sphalerite and minor galena form a pore-space filling cement.
Sorting: Poorly to moderately sorted
Intergrain relationships: Grain supported. Quartz compose matrix. Sphalerite and/or galena is occupying pore-spaces.
Textural maturity: Submature (mix of quartz grain sizes)

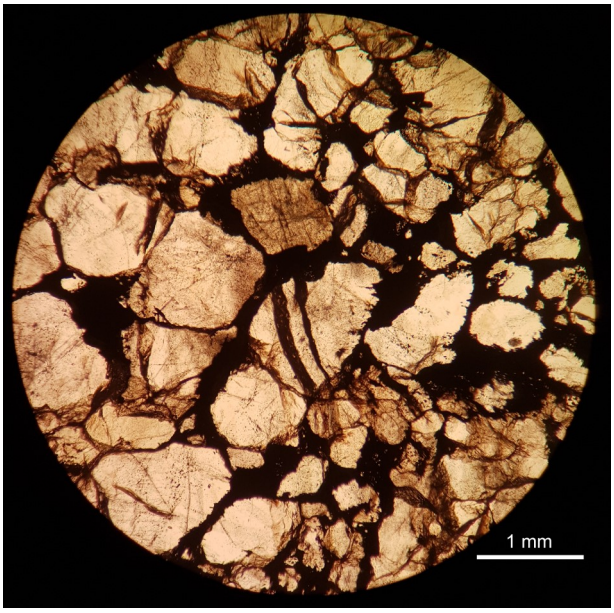

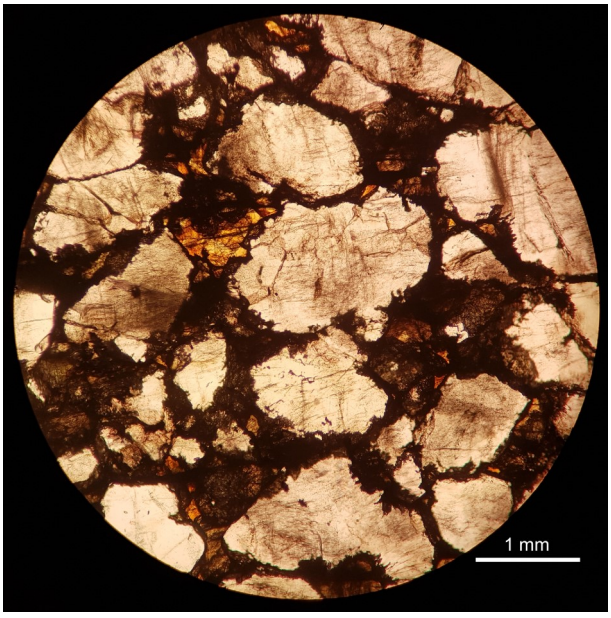

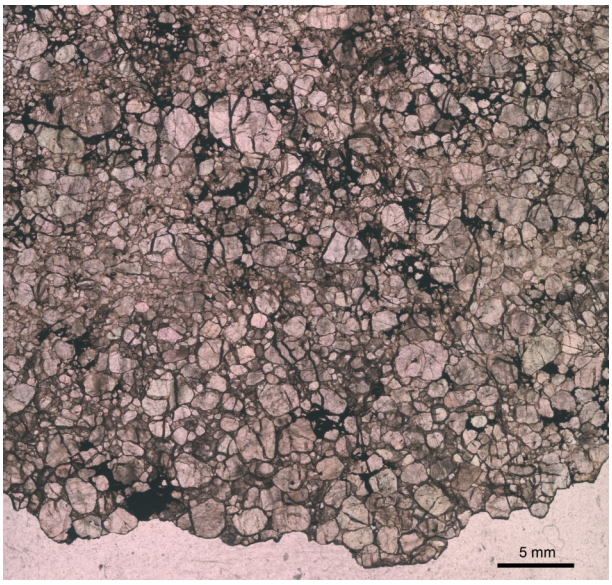

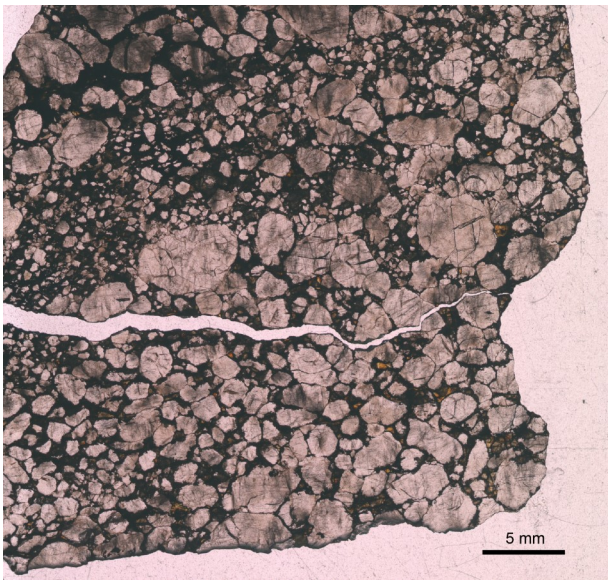

Granberget 02-09

Thin section description: Darkish sulphide mineralizations along fractures. Sub-litharenite.
Main mineralogy: Quartz, galena, sphalerite
Grain size: Equigranular, medium sized.
Grain shapes: Sub-rounded grain size.
Sorting: Well sorted.
Intergrain relationships: Quartz grains are occasionally cemented together. Mineralizations of galena occur between quartz grains and along fractures and brownish sphalerite are present in pore spaces locally.
Textural maturity: Mature.

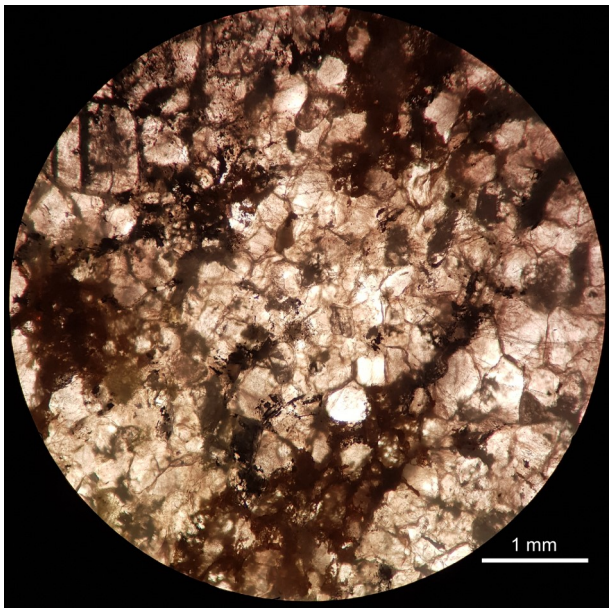

Granberget BRB 115

Thin section description: Coarse grained sandstone. Brownish sphalerite and dark grey galena mineralizations occur in fractions and as cement between the large quartz grains. Sample is richly mineralized as cement is predominantly sphalerite ± galena. Quartz grains are fractured. Thin section image is absent.
Main mineralogy: Quartz, galena, sphalerite
Grain size: Coarse grained.
Grain shapes: Sub-angular to sub-rounded.
Sorting: Well-sorted.
Intergrain relationships: Quartz grains are cemented by sphalerite and galena.
Textural maturity: Moderate.

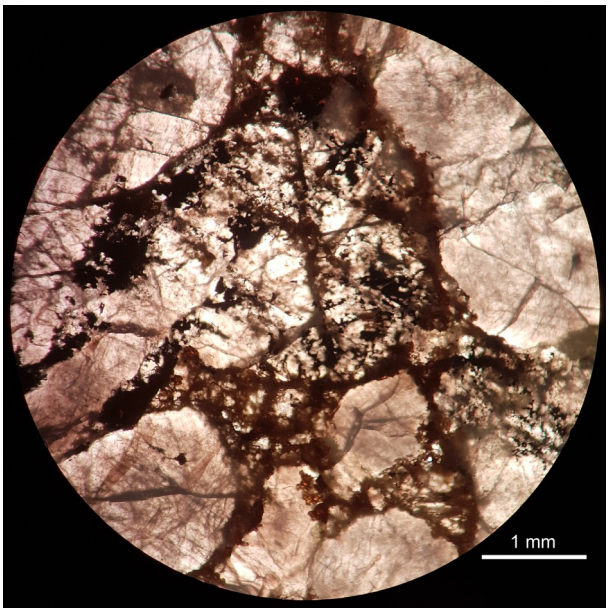

Granberget BRB 119

Thin section description: Large grain size variations, breccia type-sandstone. Sample is richly mineralized by dark grey-metallic luster galena and light brown shimmering sphalerite. Mineralization are present in large pore-spaces but also in breccia-induced fractures occasionally cross-cutting large quartz grains.
Main mineralogy: Quartz, sphalerite, galena.
Grain size: Coarse to fine grained.
Grain shapes: Angular to sub-angular.
Sorting: Poorly sorted.
Intergrain relationships: Large quartz breccia-clasts of quartz cemented with sphalerite and galena.
Textural maturity: Submature to mature.

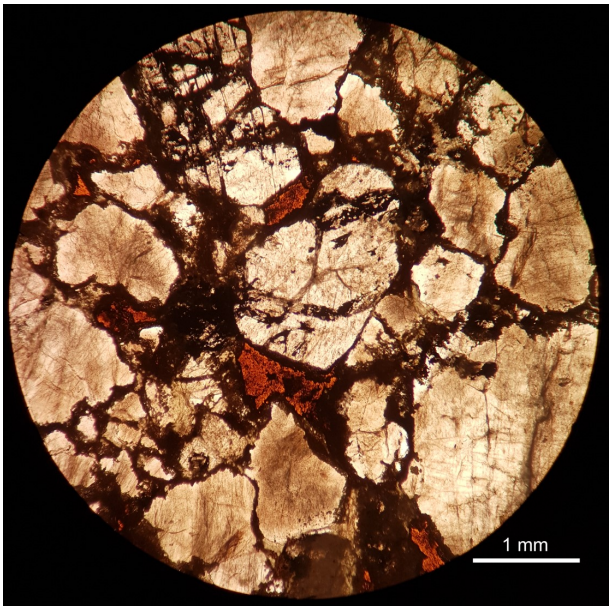

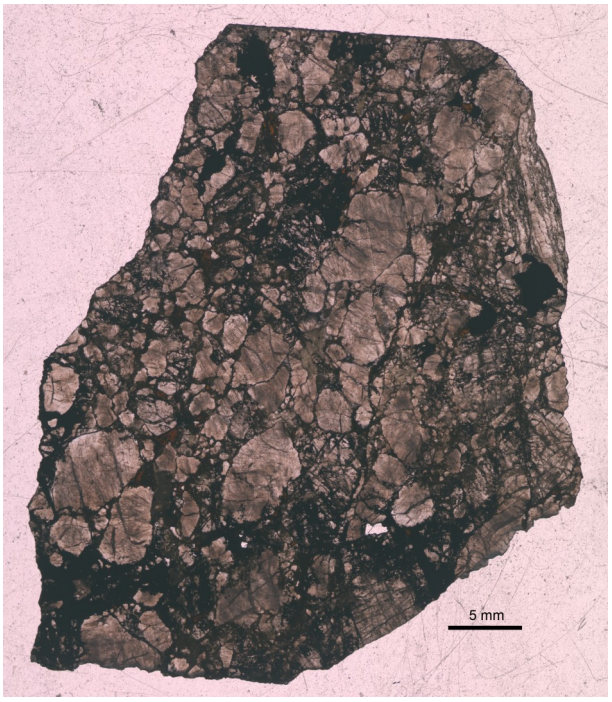

Granberget BRB 15

Thin section description: Brecciated quartz-sandstone which is mineralized by predominantly dark -grey metal-luster galena and minor dark brownish sphalerite occurring in veins. Galena is of a disseminated nature. Occasionally the ore minerals are occurring in calcite-veinlets.
Main mineralogy: Quartz, sphalerite, galena, calcite.
Grain size: Coarse to fine grained.
Grain shapes: Angular (brecciated).
Sorting: Poorly sorted.
Intergrain relationships: Brecciation, fractures cross-cutting through and between large quartz grains. Fractures are filled with galena, sphalerite and calcite.
Textural maturity: Submature to mature.

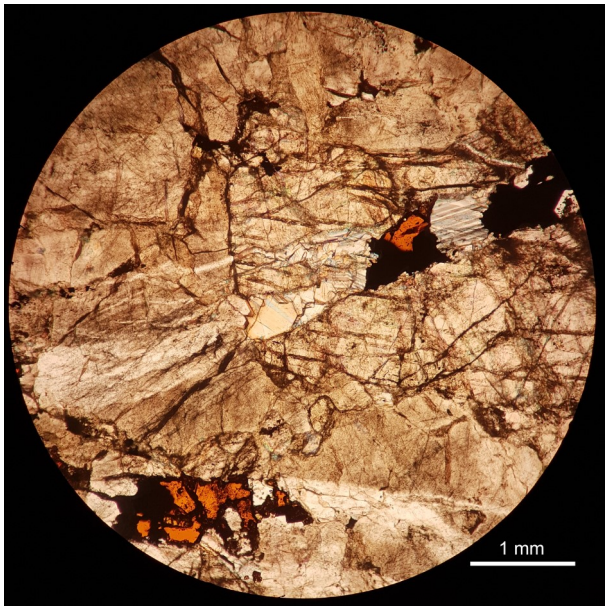

Granberget BH 74

Thin section description: Poorly sorted quartz-rich sandstone with light brownish sphalerite mineralized in a network of interstitial spaces. Galena mineralizations are more sparsely distributed as dark metallic aggregations.
Main mineralogy: Quartz , sphalerite, galena.
Grain size: Coarse to medium grained.
Grain shapes: Sub-angular.
Sorting: Moderately sorted.
Intergrain relationships: Quartz grains cemented by predominantly sphalerite and minor galena.
Textural maturity: Moderate.

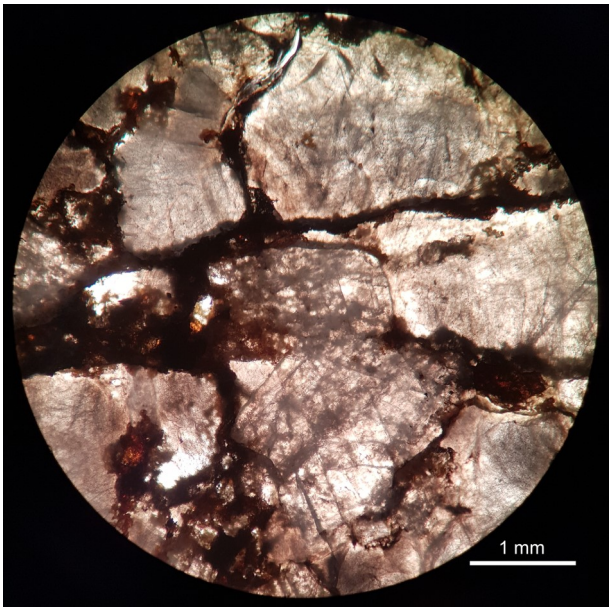

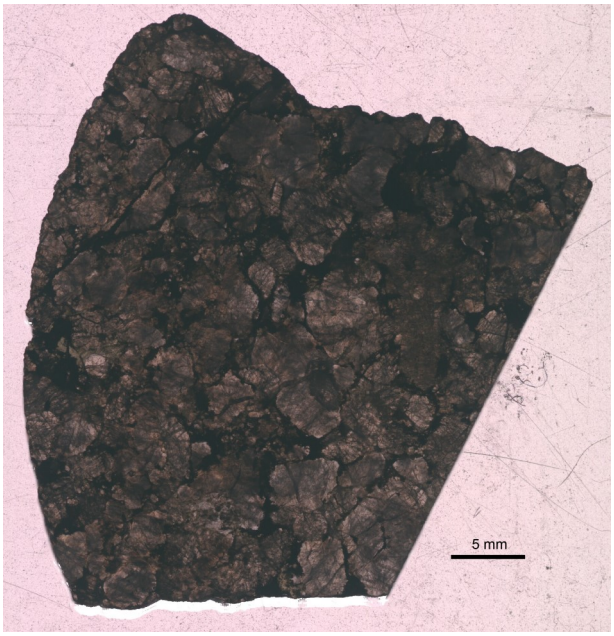

Tidigare skrifter i serien ”Examensarbeten i Geologi vid Lunds universitet”:

472. Fouskopoulos Larsson, Anna, 2016: XRF -studie av sedimentära borrkärnor - en metodikstudie av programvarorna Q-spec och Tray-sum. (15 hp)
473. Jansson, Robin, 2016: Är ERT och Tidsdomän IP potentiella karteringsverktyg inom miljögeologi? (15 hp)
474. Heger, Katja, 2016: Makrofossilanalys av sediment från det tidig-holocena undervattenslandskapet vid Haväng, östra Skåne. (15 hp)
475. Swierz, Pia, 2016: Utvärdering av vattenkemisk data från Borgholm kommun och dess relation till geologiska förhållanden och markanvändning. (15 hp)
476. Mårdh, Joakim, 2016: WalkTEM-undersökning vid Revingehed provpumpningsanläggning. (15 hp)
477. Rydberg, Elaine, 2016: Gummigranulat - En litteraturstudie över miljö- och hälsopåverkan vid användandet av gummigranulat. (15 hp)
478. Björnfors, Mark, 2016: Kusterosion och äldre kustdyners morfologi i Skälderviken. (15 hp)
479. Ringholm, Martin, 2016: Klimatutlöst matbrist i tidiga medeltida Europa, en jämförande studie mellan historiska dokument och paleoklimatarkiv. (15 hp)
480. Teilmann, Kim, 2016: Paleomagnetic dating of a mysterious lake record from the Kerguelen archipelago by matching to paleomagnetic field models. (15 hp)
481. Schönström, Jonas, 2016: Resistivitets- och markradarmätning i Ängelholmsområdet - undersökning av korrosiva markstrukturer kring vattenledningar. (15 hp)
482. Martell, Josefin, 2016: A study of shock-metamorphic features in zircon from the Siljan impact structure, Sweden. (15 hp)
483. Rosvall, Markus, 2016: Spår av himlakroppskollisioner - bergarter i nedslagskratrar med fokus på Mien, Småland. (15 hp)
484. Olausson, My, 2016: Resistivitets- och IP -mätningar på den nedlagda deponin Gustavsfält i Halmstad. (30 hp)
485. Plan, Anders, 2016: Markradar- och resistivitetsmätningar – undersökningar utav korrosionsförhöjande markegenskaper kring fjärrvärmeledningar i Ängelholm. (15 hp)
486. Jennerheim, Jessica, 2016: Evaluation of methods to characterise the geochemistry of limestone and its fracturing in connection to heating. (45 hp)
487. Olsson, Pontus, 2016: Ekologiskt vatten från Lilla Klåveröd: en riskinventering för skydd av grundvatten. (15 hp)
488. Henriksson, Oskar, 2016: The Dynamics of Beryllium 10 transport and deposition in lake sediments. (15 hp)
489. Brådenmark, Niklas, 2016: Lower to Middle Ordovician carbonate sedimentology and stratigraphy of the Pakri peninsula, north-western Estonia. (45 hp)
490. Karlsson, Michelle, 2016: Utvärdering av metoderna DCIP och CSIA för identifiering av nedbrytningszoner för klorerade lösningsmedel: En studie av Färgaren 3 i Kristianstad. (45 hp)
491. Elali, Mohammed, 2016: Flygsanddyners inre uppbyggnad – georadarundersökning. (15 hp)
492. Preis-Bergdahl, Daniel, 2016: Evaluation of DC Resistivity and Time-Domain IP Tomography for Bedrock Characterisation at Önneslöv, Southern Sweden. (45 hp)
493. Kristensson, Johan, 2016: Formation evaluation of the Jurassic Stø and Nordmela formations in exploration well 7220/8-1, Barents Sea, Norway. (45 hp)
494. Larsson, Måns, 2016: TEM investigation on Challapampa aquifer, Oruro Bolivia. (45 hp)
495. Nylén, Fredrik, 2017: Utvärdering av borrhålskartering avseende kalksten för industriella ändamål, File Hajdarbrottet, Slite, Gotland. (45 hp)
496. Mårdh, Joakim, 2017: A geophysical survey (TEM; ERT) of the Punata alluvial fan, Bolivia. (45 hp)
497. Skoglund, Wiktor, 2017: Provenansstudie av detriala zirkoner från ett guldförande alluvium vid Ravlunda skjutfält, Skåne. (15 hp)
498. Bergcrantz, Jacob, 2017: Ett fönster till Kattegatts förflutna genom analys av bottenlevande foraminiferer. (15 hp)
499. O'Hare, Paschal, 2017: Multiradionuclide evidence for an extreme solar proton event around 2610 BP. (45 hp)
500. Goodship, Alastair, 2017: Dynamics of a retreating ice sheet: A LiDAR study in Värmland, SW Sweden. (45 hp)
501. Lindvall, Alma, 2017: Hur snabbt påverkas och nollställs luminiscenssignaler under naturliga ljusförhållanden? (15 hp)
502. Sköld, Carl, 2017: Analys av stabila isotoper med beräkning av blandningsförhållande i ett grundvattenmagasin i Älvkarleby-Skutskär. (15 hp)
503. Sällström, Oskar, 2017: Tolkning av geofysiska mätningar i hammarborrhål på södra Gotland. (15 hp)
504. Ahrenstedt, Viktor, 2017: Depositional

history of the Neoproterozoic Visingsö Group, south-central Sweden. (15 hp)

505. Schou, Dagmar Juul, 2017: Geometry and faulting history of the Long Spur fault zone, Castle Hill Basin, New Zealand. (15 hp)
506. Andersson, Setina, 2017: Skalbärande marina organismer och petrografi av tidigcampanska sediment i Kristianstadsbassängen – implikationer på paleomiljö. (15 hp)
507. Kempengren, Henrik, 2017: Föroreningsspridning från kustnära deponi: Applicering av Landsim 2.5 för modellering av lakvattentransport till Östersjön. (15 hp)
508. Ekborg, Charlotte, 2017: En studie på samband mellan jordmekaniska egenskaper och hydrodynamiska processer när erosion påverkar släntstabiliteten vid ökad nederbörd. (15 hp)
509. Silvén, Björn, 2017: LiDARstudie av glaciala landformer sydväst om Söderåsen, Skåne, Sverige. (15 hp)
510. Rönning, Lydia, 2017: Ceratopsida dinosauriers migrationsmönster under krittiden baserat på paleobiogeografi och fylogeni. (15 hp)
511. Engleson, Kristina, 2017: Miljökonsekvensbeskrivning Revinge brunnsfält. (15 hp)
512. Ingered, Mimmi, 2017: U-Pb datering av zirkon från migmatitisk gnejs i Delsjöområdet, Idefjordenterrängen. (15 hp)
513. Kervall, Hanna, 2017: EGS - framtidens geotermiska system. (15 hp)
514. Walheim, Karin, 2017: Kvartsmineralogins betydelse för en lyckad luminiscensdatering. (15 hp)
515. Aldenius, Erik, 2017: Lunds Geotermisystem, en utvärdering av 30 års drift. (15 hp)
516. Aulin, Linda, 2017: Constraining the duration of eruptions of the Rangitoto volcano, New Zealand, using paleomagnetism. (15 hp)
517. Hydén, Christina Engberg, 2017: Drumlinerna i Löberöd - Spår efter flera isrörelseriktningar i mellersta Skåne. (15 hp)
518. Svantesson, Fredrik, 2017: Metodik för kartläggning och klassificering av erosion och släntstabilitet i vattendrag. (45 hp)
519. Stjern, Rebecka, 2017: Hur påverkas luminiscenssignaler från kvarts under laboratorieförhållanden? (15 hp)
520. Karlstedt, Filippa, 2017: P-T estimation of the metamorphism of gabbro to garnet amphibolite at Herrestad, Eastern Segment of the Sveconorwegian orogen. (45 hp)
521. Önnervik, Oscar, 2017: Ooider som naturliga arkiv för förändringar i havens geokemi och jordens klimat. (15 hp)
522. Nilsson, Hanna, 2017: Kartläggning av sand och naturgrus med hjälp av resistivitetsmätning på Själland, Danmark. (15 hp)
523. Christensson, Lisa, 2017: Geofysisk undersökning av grundvattenskydd för planerad reservvattentäkt i Mjölkalånga, Hässleholms kommun. (15 hp)
524. Stamsnijder, Joaen, 2017: New geochronological constraints on the Klipriviersberg Group: defining a new Neoarchean large igneous province on the Kaapvaal Craton, South Africa. (45 hp)
525. Becker Jensen, Amanda, 2017: Den eocena Furformationen i Danmark: exceptionella bevaringstillstånd har bidragit till att djurs mjukdelar fossiliserats.(15 hp)
526. Radomski, Jan, 2018: Carbonate sedimentology and carbon isotope stratigraphy of the Tallbacken-1 core, early Wenlock Slite Group, Gotland, Sweden. (45 hp)
527. Pettersson, Johan, 2018: Ultrastructure and biomolecular composition of sea turtle epidermal remains from the Campanian (Upper Cretaceous) North Sulphur River of Texas. (45 hp)
528. Jansson, Robin, 2018: Multidisciplinary perspective on a natural attenuation zone in a PCE contaminated aquifer. (45 hp)
529. Larsson, Alfred, 2018: Rb-Sr sphalerite data and implications for the source and timing of Pb-Zn deposits at the Caledonian margin in Sweden. (45 hp)

LUNDS UNIVERSITET

Geologiska institutionen
Lunds universitet
Sölvegatan 12, 223 62 Lund